ERDC/CRREL TR-15-14

US Army Corps
of Engineers®
Engineer Research and
Development Center

ERDC
INNOVATIVE SOLUTIONS
for a safer, better world

*ERDC Center-Directed Research*

# Imaging of Ground Ice with Surface-Based Geophysics

Kevin Bjella, Steve Arcone, and Thomas Douglas

October 2015

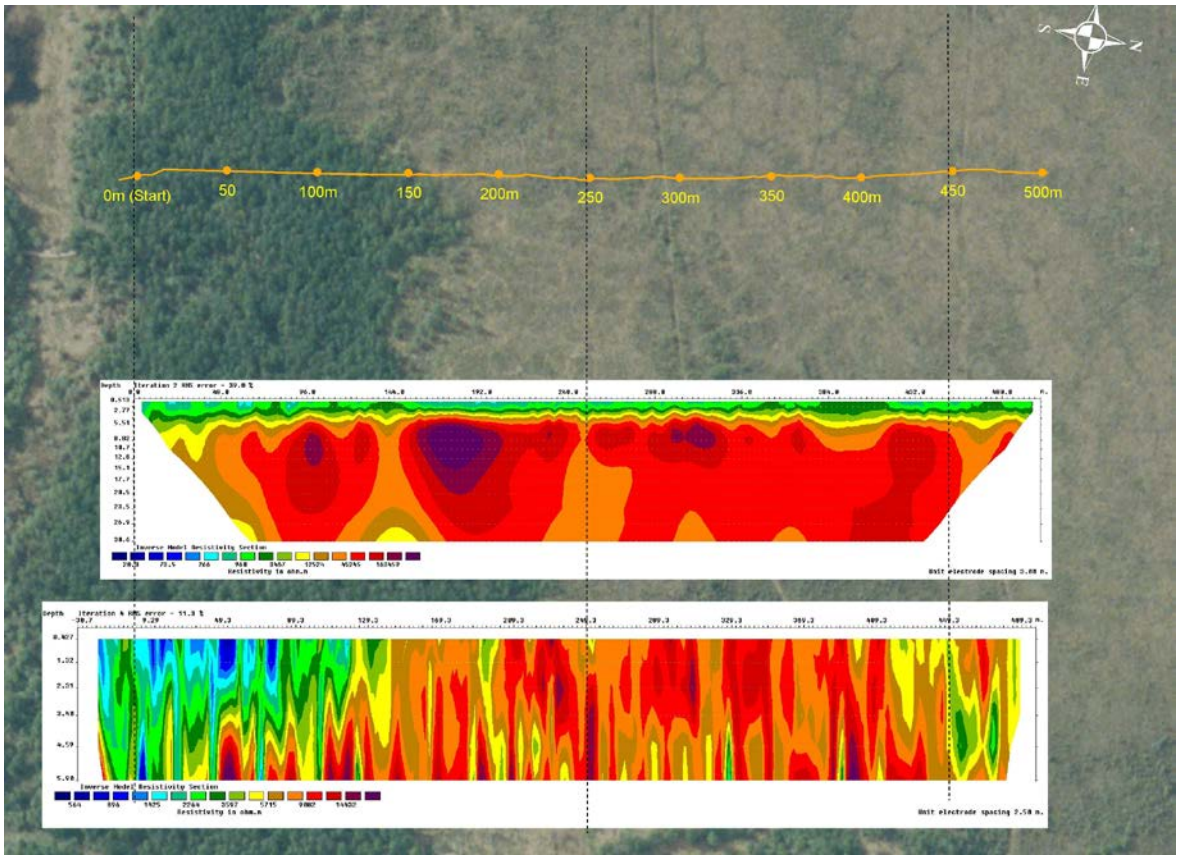


Cold Regions Research
and Engineering Laboratory

**The U.S. Army Engineer Research and Development Center (ERDC)** solves the nation's toughest engineering and environmental challenges. ERDC develops innovative solutions in civil and military engineering, geospatial sciences, water resources, and environmental sciences for the Army, the Department of Defense, civilian agencies, and our nation's public good. Find out more at www.erdc.usace.army.mil.

To search for other technical reports published by ERDC, visit the ERDC online library at http://acwc.sdp.sirsi.net/client/default.

ERDC/CRREL TR-15-14
October 2015

# Imaging of Ground Ice with Surface-Based Geophysics

Kevin Bjella and Thomas Douglas

*U.S. Army Engineer Research and Development Center (ERDC)*
*Cold Regions Research and Engineering Laboratory (CRREL)*
*Alaska Projects Office*
*Building 4070, 9th Street*
*Fort Wainwright, AK 99703*

Steve Arcone

*U.S. Army Engineer Research and Development Center (ERDC)*
*Cold Regions Research and Engineering Laboratory (CRREL)*
*72 Lyme Road*
*Hanover, NH 03755-1290*

Final Report



Prepared for Headquarters, U.S. Army Corps of Engineers
Washington, DC 20314-1000

Under ERDC Center-Directed Research project “Integrated Technologies for Delineating Permafrost and Ground-State Conditions”

# Abstract

Electrical properties of earth materials have profound differences due to the phase change of water to ice. This contrast is useful when using electro-magnetic methods to study permafrost terrains where frozen and thawed materials are intermixed. Engineering and science are in need of efficient, non-invasive tools for imaging ice and sediment composition. Borehole information is often used to map ice in permafrost terrains; but it is time consuming, expensive, and can lead to over- or underquantification of ground ice. Advances in computing power have led to refined surface-based geophysical methods, and the goal of this study was to determine if the latest commercial technologies or system were promising for imaging ground ice and associated features and to compare the results across a variety of permafrost terrains.

Electrical Resistivity Tomography (ERT), in particular, has been effective for imaging ground ice. ERT measures the ability of materials to conduct or resist an electric current. A variation of this method, capacitive coupled resistivity (CCR) offers the ability for continuous data collection while moving across the landscape at scales of meters to kilometers. This greatly enhances the cost efficiency, applicability, and overall usefulness of the techniques and provides the ability to view variations in permafrost ice content on these larger scales.

# Contents

# Illustrations

## Figures

# Preface

This study was conducted for the U.S. Army Engineer Research and Development Center (ERDC) Center-Directed Research Program under the project "Integrated Technologies for Delineating Permafrost and Ground-State Conditions."

The work was performed by Kevin Bjella (Force Projection and Sustainment Branch, Dr. Loren Wehmeyer, Acting Chief), Dr. Steven A. Arcone, (Signature Physics Branch, Dr. Loren Wehmeyer, Acting Chief), and Dr. Thomas A. Douglas, (Biogeochemical Sciences Branch, Dr. Justin Berman, Chief), U.S. Army Engineer Research and Development Center, Cold Regions Research and Engineering Laboratory (ERDC-CRREL). At the time of publication, Dr. Loren Wehmeyer was Chief of the Research and Engineering Division. The Deputy Director of ERDC-CRREL was Dr. Lance Hansen, and the Director was Dr. Robert Davis.

COL Bryan S. Green was the Commander of ERDC, and Dr. Jeffery P. Holland was the Director.

# Acronyms and Abbreviations

| | |
|---|---|
| 2-D | 2-Dimensional |
| 3-D | 3-Dimensional |
| APRS | Alaska Permafrost Research Station |
| CCR | Capacitive Coupled Resistivity |
| CRREL | Cold Regions Research and Engineering Laboratory |
| DEM | Digital Elevation Model |
| DPT | Direct Push Technology |
| ERDC | U.S. Army Engineer Research and Development Center |
| ERT | Electrical Resistivity Tomography |
| GPS | Global Positioning System |
| LiDAR | Light Detection and Ranging |
| SIPRE | Snow, Ice, and Permafrost Research Establishment |
| T1 | Transect 1 |
| T2 | Transect 2 |

# 1 Background

## 1.1 Introduction

Permanently frozen ground, or permafrost, underlies 22.8 million km$^2$ (one-quarter) of the northern hemisphere's land area (Zhang et al. 2003). Permafrost is soil and rock that remains frozen for two or more consecutive years. This implies that permafrost is strictly defined by temperature alone. However, near-surface earth materials are often associated with and affected by surface water and groundwater. Consequently, permafrost in most regions of the planet is associated with quantities of ground ice, often to great extents, and most often with massive ice features, which can compose 50% to 70% of the total bulk soil volume (Bray et al. 2006; Kanevskiy et al. 2011). This ground ice is of extreme interest to engineers and scientists in many fields of practice and study.

Surface-based geophysical techniques have been used in the past few decades to measure ground ice, but widespread use is limited. Studies have determined the effectiveness of the various methods for detecting and mapping seasonally and permanently frozen ground (Lewkowicz et al. 2011; Kneisel et al. 2008); however, no one has conducted a study to determine the accuracy of expedient resistivity methods. The purpose of our project was to ascertain if available geophysical measurement techniques can accurately and efficiently measure or detect the presence of ground ice, especially to the degree that would provide useful information to guide engineering design.

## 1.2 Permafrost terrain characteristics

### 1.2.1 Ground ice

There are two processes for permanent ground freezing. Epigenetic freezing occurs to a column of material previously existing in the thawed state. Syngenetic freezing occurs during the sedimentation process, where newly deposited sediment is incrementally added to the top of the permafrost table (Shur et al. 2004). Ground and surface water greatly influence these processes. Ground-ice extent and type are functions of the rate of sediment accumulation and erosion, while the thickness and extent of the ice features are governed by the freezing rate and repeated processes. When a soil column exists in the thawed state, the moisture content is rarely above

saturation and often can be undersaturated. On freezing, this will generally result in ice-moderate to ice-poor epigenetic permafrost. Because syngenetic permafrost is due to the incremental addition of minute layers of sediment to the top of the permafrost, not only is the new increment at a saturated or undersaturated condition, there generally is a minute layer of segregation ice created with each aggraded layer. This process results in ice-rich to super ice-rich sediment, also called ice complex or yedoma.

*Matrix ice* is created by the freezing of interstitial water within sediment and fractured rock. Frozen, undersaturated conditions are generally considered ice-poor to ice-moderate, while frozen saturated and supersaturated conditions are ice-moderate to ice-rich (Williams and Smith 1989).

*Segregation ice* is created in conjunction with the freezing isotherm of an advancing freezing front. This typically occurs during seasonal freezing events, but segregation ice also occurs during refreezing of thermo-eroded permafrost structures (Shur et al. 2005). This ice can be from millimeters to centimeters thick and millimeters to tens of meters long.

*Wedge ice* is an intrusive ice feature occurring in existing permafrost terrain when surface water infiltrates into downward-propagated contraction cracks originating at the surface from extreme cold-air events. The process tends to repeat adjacent to previously initiated zones, resulting in lateral aggradation of ice layers with characteristic wedge geometry. This ice is typically meters in vertical extent, up to 3 to 4 m wide at the surface, and tens of meters in length (Figure 1).

*Ice complex (yedoma)* is a term for fine-grained air-fall and slope-wash material that became permafrost syngenetically. Millimeter thickness segregation ice is created during the freezing process, and this segregation ice ultimately can make up to 60% to 70% of the bulk volume of the soil column (Kanevskiy et al. 2008). Within this very ice-rich sediment, wedge ice is almost always associated with this type of terrain and can extend the entire length of the soil column and can be up to 3 to 4 m in width.

Figure 1. Ice wedges (*white features*) excavated in permafrost at Thule Air Base in Greenland in the 1960s. (Photo by A. E. Corte, SIPRE [Snow, Ice, and Permafrost Research Establishment].)

### 1.2.2 Active layer

Soil and rock at the surface extending down to the top of the permafrost (permafrost table) that thaws in the summer is the seasonally thawed *active layer* (French 1976). A significant feature of the active layer is that the active-zone water typically pools at the depth of maximum thaw, often on the permafrost table. Another significant feature is the transition zone (Shur et al. 2005), which exists between the seasonally thawed layer and the permafrost table below. This transition zone is typically host to layers of segregation ice often exceeding many centimeters in thickness. This zone typically will thaw over sub-decadal to multi-centennial time scales. However, the temperature regime (winter and summer), precipitation, soil pore-water migration, vegetation, and topography define the location of this region from year to year.

Winter freezing of the soil pore water creates segregation at the top of the permafrost table, which may remain for many years, particularly where the seasonal variation in climate prevents complete thaw of the transition zone (Shur et al. 2005). The active layer is also host to matrix ice and the initial ice veins of wedge ice. However, these are destroyed by thaw every year unless significant aggradation of the permafrost table occurs or other thermal-regime alteration occurs preventing thawing of this ice. Typical active-layer depths at our study sites are 40 to 100 cm, and they are predominantly controlled by soil and vegetation type and the ice content of the soil.

# 2 Field Sites and Measurements

## 2.1 Field locations

Our team established three test sites in the vicinity of Fairbanks, AK (Figure 2). At each site, we established a linear transect, a 2 m wide line cut through the vegetation, and conducted a high resolution Global Positioning System (GPS) survey to establish the ground topography. The transects were sighted to cross the most varied terrain possible.

Figure 2. Locations of the three study sites in the vicinity of Fairbanks, AK.

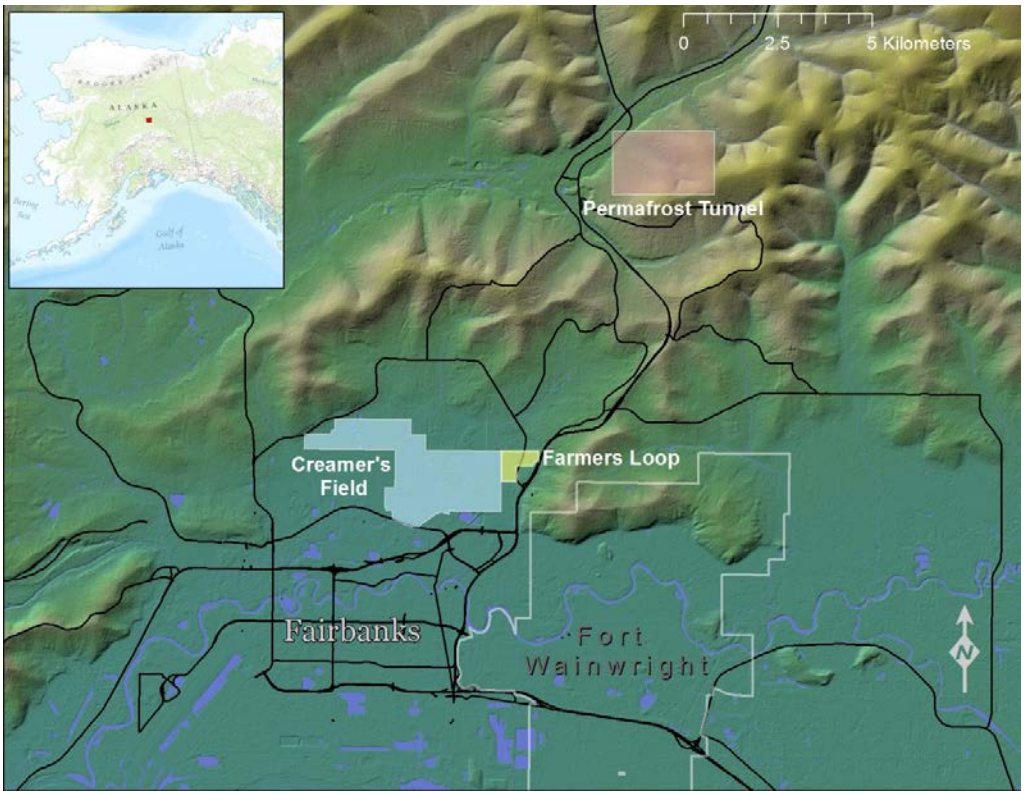


At the State of Alaska, Creamer's Field Migratory Refuge, we established a 500 m long transect through polygonal ground. At the U.S. Army Engineer Research and Development Center, Cold Region Research and Engineering Laboratory (ERDC-CRREL), Farmers Loop Experimental Station, we surveyed two parallel 400 m long transects. At the ERDC-CRREL Permafrost Tunnel, we established a 400 m long transect was established. In addition to the surface geophysical surveys we performed, the transects have also been the focus of other collaborative measurements and studies, including

- vegetation mapping,
- vegetation spectral-reflectance measurements,
- active-layer depth measurements,
- air and soil temperature monitoring,
- shallow and deep borehole drilling,
- snow depth studies,
- airborne remote sensing, and
- satellite remote sensing.

### 2.1.1 Farmers Loop

The primary location used for these studies was the ERDC-CRREL Alaska Permafrost Research Station (APRS)–Farmers Loop Road study site, located on the northeast side of Fairbanks (Figure 3). Transect 1 (T1) and Transect 2 (T2) were 400 m in length and started near a major four-lane paved roadway (Farmers Loop Road) heading west-northwest.

Figure 3. An airborne LiDAR (light detection and ranging) image of the Farmers Loop site collected in May 2014. The *upper yellow line* denotes T1, and the *lower line* denotes T2. Both transects are 400 m long. Note the presence of polygonal ground toward the far ends of both transects. Also note Farmers Loop Road (to the right of the image) and the presence of ponds and two skiing and hiking trails that show up as linear (north–south) features in the image. North is at the top.

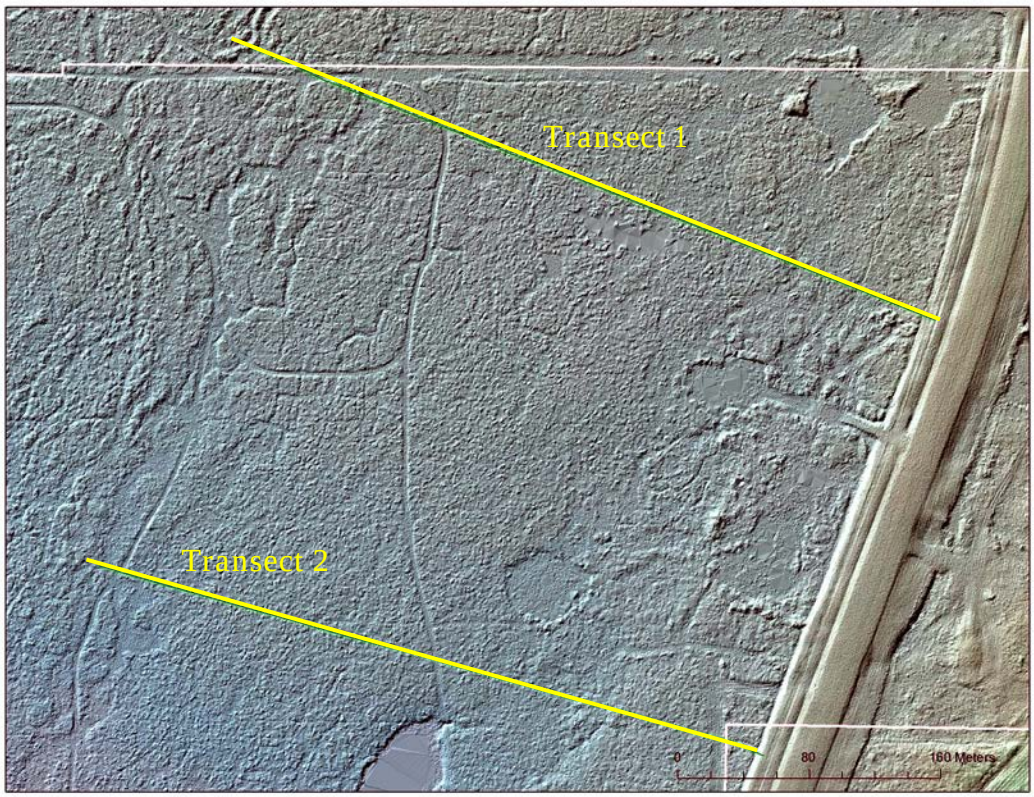

The transects were parallel to each other, separated by 290 m. Each transect began in a mixed deciduous and coniferous forest with degrading permafrost (thermokarst) and intermittent standing surface water. At approximately 80 m, the vegetation changed to a poorly drained mixed tussock and dwarf deciduous forest. At approximately 350 m, the transects extend into a mixed dwarf and full-standing coniferous forest of sphagnum moss (Figure 4). Figure 5 and Figure 6 present results from seasonal thaw measurements along the two transects.

Figure 4. Photos depicting the main vegetation and terrain characteristics along the two Farmers Loop transects.

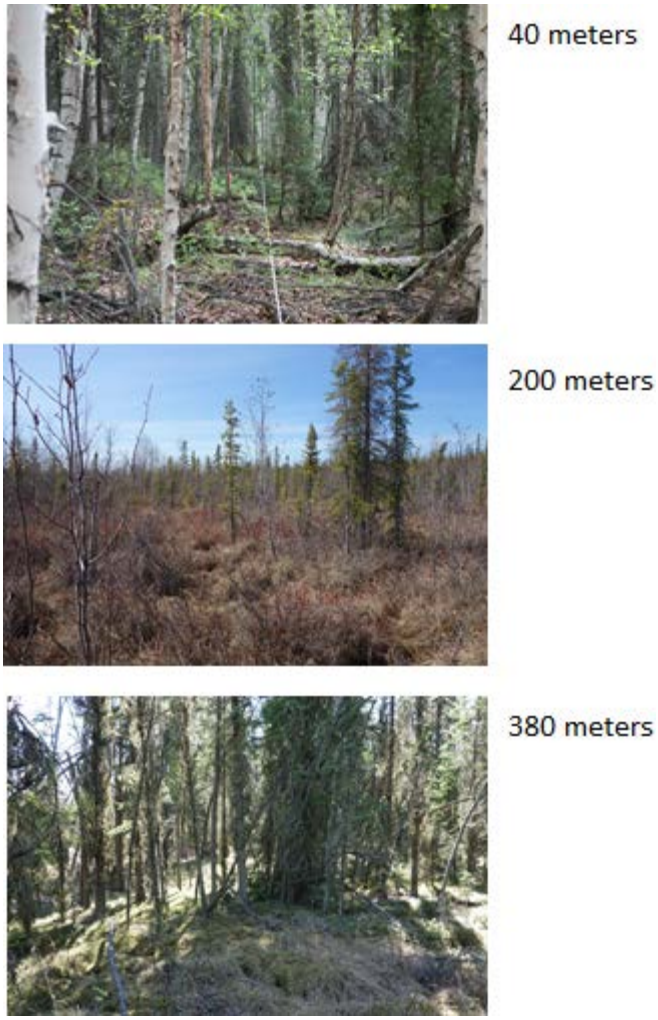

Figure 5. Results from frost probe measurements of the seasonally thawed active layer along Farmers Loop T1.

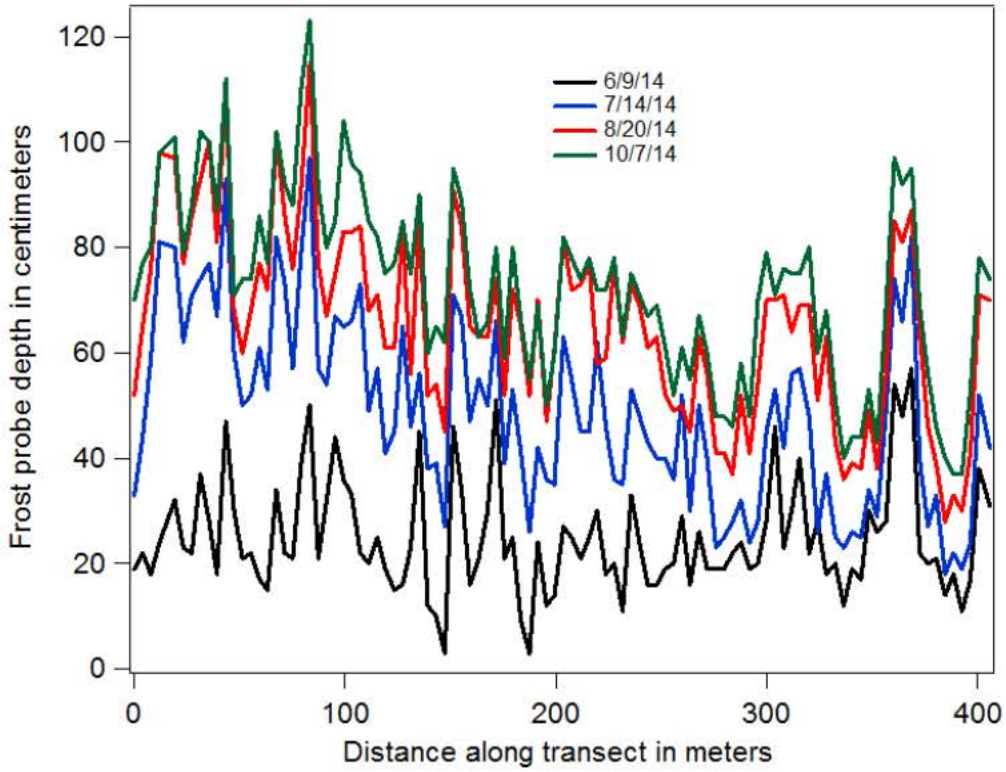


Figure 6. Results from frost probe measurements of the seasonally thawed active layer along Farmers Loop T2.

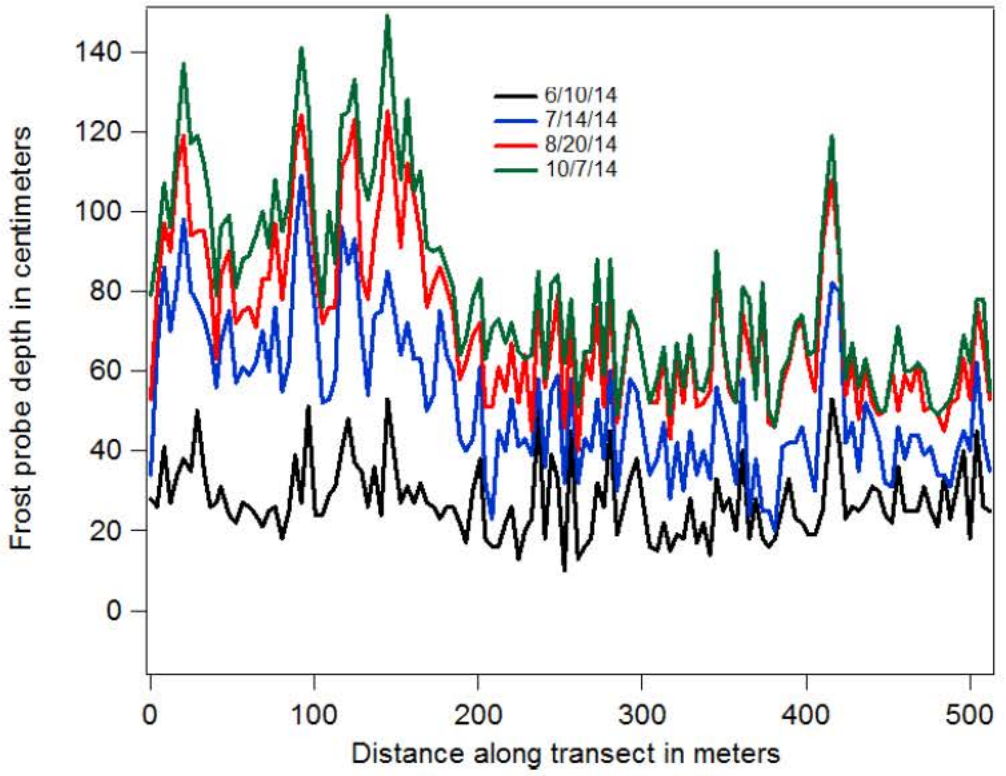

Little information was known about the geocryology of this site prior to our study. Péwé (1975) suggested that the site consists of ice-rich reworked loess deposited at the base of Birch Hill .This material was most likely deposited by alluvial action of Isabella Creek or the associated tributaries in the near vicinity, such as the Chena River. Well borings from the 1950s suggested gravel at a depth 90 m and bedrock at 140 m. CRREL infrastructure located on the site (on the east side of Farmers Loop Road) from 1946 to the early 1990s has suffered from thaw settlement issues, and significant thermokarst can be seen directly west of Farmers Loop Road where historical pile testing and pavement color testing was performed.

### 2.1.2 Creamer's Field

We constructed one transect at this site, which is located north of Fairbanks, AK, in the State of Alaska Migratory Waterfowl Refuge (Figure 7).

Figure 7. An airborne LiDAR image of the Creamer's Field site collected in May 2014. The *yellow line* denotes the location of the 500 m long transect. Note the presence of polygonal ground throughout the transect. Toward the beginning of the transect (the bottom of the image), the polygons are approximately 5 m across and are more vertically varied than they are further out the transect. Two skiing and hiking trails show up as linear (east–west) features in the image.

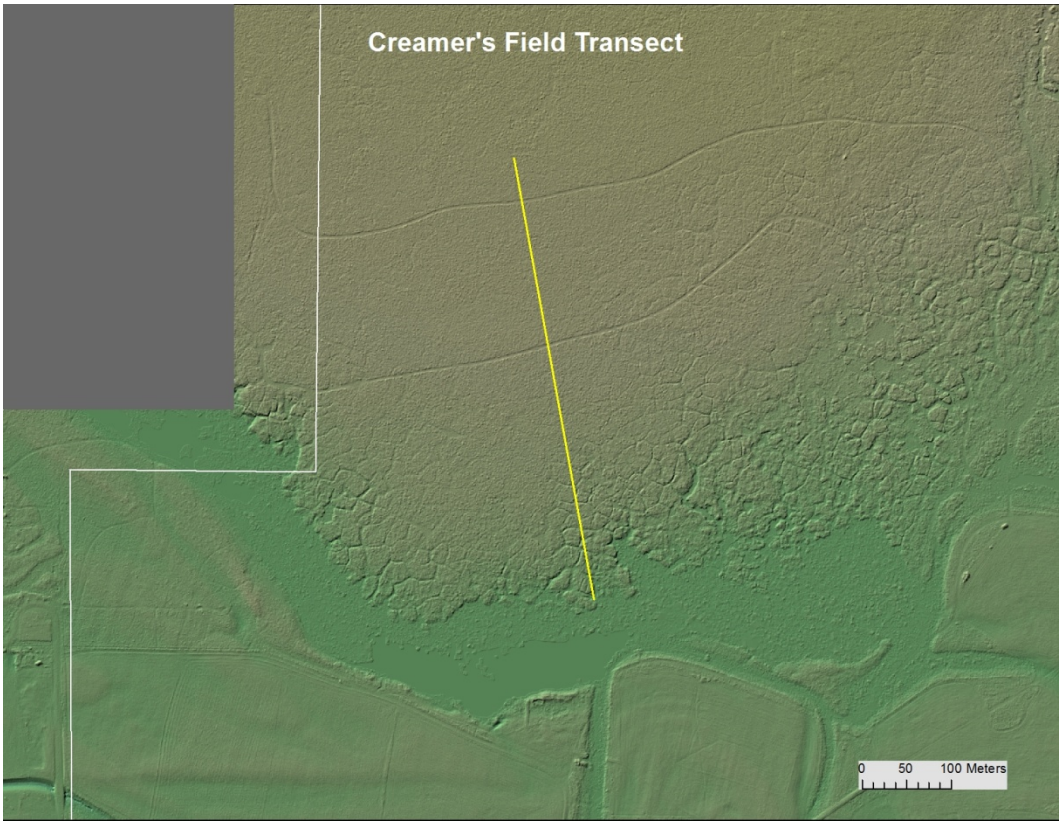

This 500 m long transect began in a mixed tall deciduous and conifer forest with thermokarst and early season standing water and was oriented to the north-northwest. At approximately 160 m, the transect transitioned to a poorly drained tussock-sedge environment; and at 300 m, dwarf deciduous and coniferous forest began, although sparsely (Figure 8). Figure 9 presents results from seasonal thaw measurements along the Creamer's Field transect.

CRREL studies from the 1960s and 1970s provided some limited knowledge of the geocryology of this site. We theorized that the area north of the site consisted of ice-rich reworked loess deposited from the hills north of Fairbanks. The thermokarst area noted earlier was immediately indicative of ice-wedge polygonal ground, typical of ice-rich, fine-grained soils of Interior Alaska. Noyes Slough, a bypass channel of the Chena River, is approximately 2 km south of the beginning of the transect. This slough, which is related to the Chena River, is typically associated with predominantly gravel sediments derived from the bed load of the Tanana River. We expect frozen gravels at unknown depth along the transect, with a possible transition to predominant gravels at the south end of the transect in an area just prior to the thermokarst area.

Figure 8. Photos depicting the main vegetation and terrain characteristics along the Creamer's Field transect.

0-140 meters

200-500 meters

Figure 9. Results from frost probe measurements of the seasonally thawed active layer along the Creamer's Field transect.

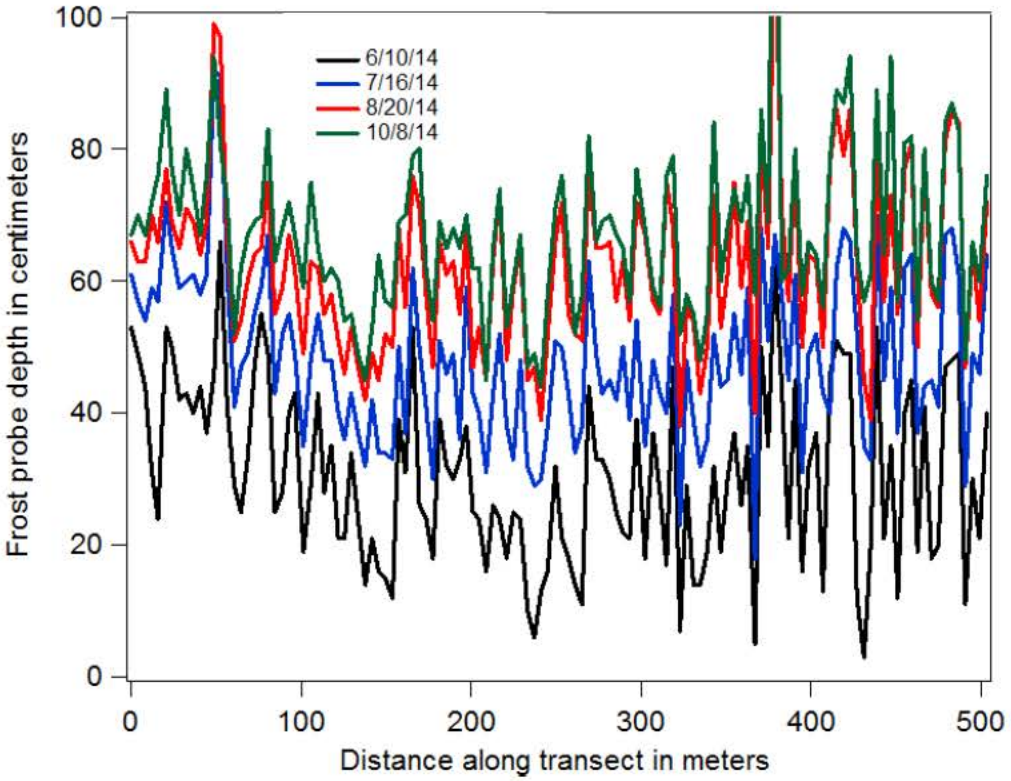


### 2.1.3 Permafrost Tunnel

We established another study site at the ERDC-CRREL APRS Permafrost Tunnels in Fox, AK, approximately 20 km north of Fairbanks (Figure 10). We established a 400 m long transect beginning in dwarf coniferous (black spruce—*Picea mariana)* with a sphagnum moss understory. At approximately 150 m, the transect emerged into a grassy, poorly drained area of the Glenn Creek drainage with intermittent sedge tussocks (Figure 11). Figure 12 presents results from seasonal thaw measurements along the Permafrost Tunnel transect.

This area has been intensively drilled and tunneled; and therefore, a great deal of geocryology is known. The site consists of approximately 4 m of ice-poor, Holocene-age, reworked, fine-grained sediment (reworked loess) overlying approximately 12 to 15 m of Pleistocene-age, very ice-rich, air-fall and reworked loess with significant wedge ice structures meters in width and tens of meters in depth (Figure 13 and Figure 14). This overlies approximately 3 m of auriferous ice-poor gravels; and these in turn overlie the Fairbanks Schist (Hamilton et al. 1988), which is often highly mechanically and chemically weathered within meters of its paleosurface.

Figure 10. An airborne LiDAR image of the Permafrost Tunnel site collected in May 2014. The *yellow line* denotes the location of the 400 m long transect.

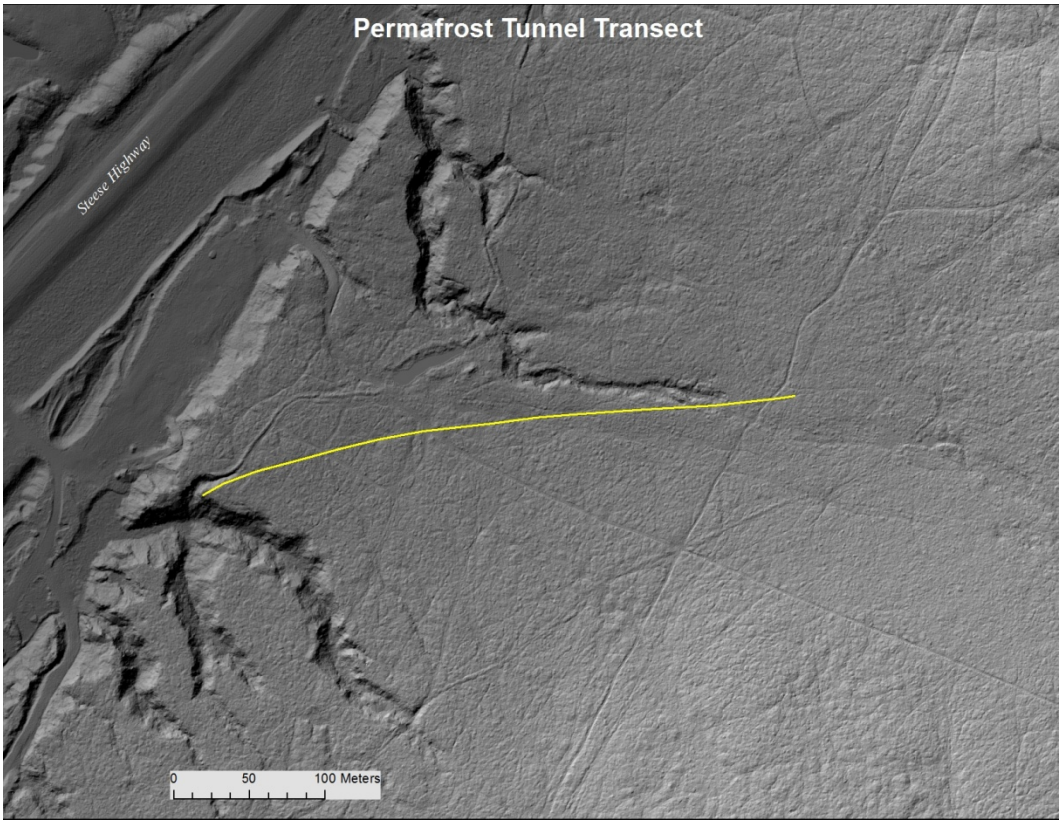


Figure 11. A photo depicting the main vegetation and terrain characteristics along the Permafrost Tunnel transect.

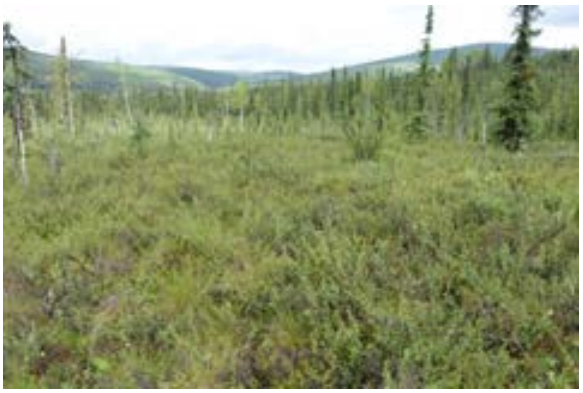

Figure 12. Results from frost probe measurements of the seasonally thawed active layer along the Permafrost Tunnel transect.

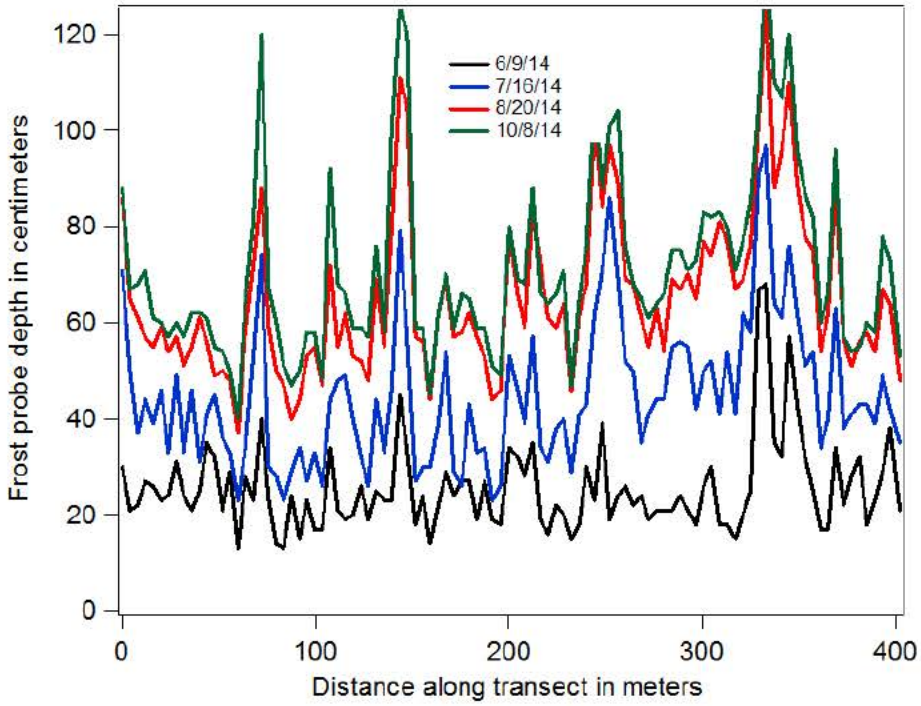


Figure 13. Wedge ice on the wall and ceiling of the new CRREL Permafrost Tunnel.

Figure 14. A road cut near the CRREL Permafrost Tunnel in the 1980s. Ice-rich Pleistocene sediments are seen adjoining wedge ice (*dark areas*). (Photo by S. Arcone, CRREL.)

## 2.2 Geophysical techniques

### 2.2.1 Electrical resistivity tomography (ERT)

Frozen earth materials, especially those with appreciable ground-ice content, are resistive to electric current flow. Resistivity has been proven to delineate between frozen and thawed and ice-rich and ice-poor terrain. To process the data, we used an inversion process included in the RES2D software package developed by Geotomosoft Solutions; and the output provided a cross section (pseudo-section) of subsurface resistivity (x, z). Our study used the Advanced Geosciences Inc., Super Sting R-8 system. In this method, electrical resistivity is measured by injecting current (galvanic) into the subsurface via two current electrodes and reading the resultant voltage via two potential electrodes (Figure 15). By measuring the current and voltage and the geometry of the electrodes, one can calculate the resistivity of the subsurface. Averaging algorithms are then used to calculate the apparent resistivity over a range of depths along an electrode line. This system is time consuming to set as the electrodes must be hammered into the subsurface, and each survey is limited to the length of the cables at maximum electrode spacing. Surveys can use different measurement geometries and different electrode pair separation distance for altering the overall survey depth and resolution. Generally, one of two techniques is utilized: the Wenner Array or Dipole-Dipole.

Figure 15. Electrical resistivity arrays: Wenner and dipole-dipole. The A–B electrodes are the current, and the M–N electrodes are the potential.

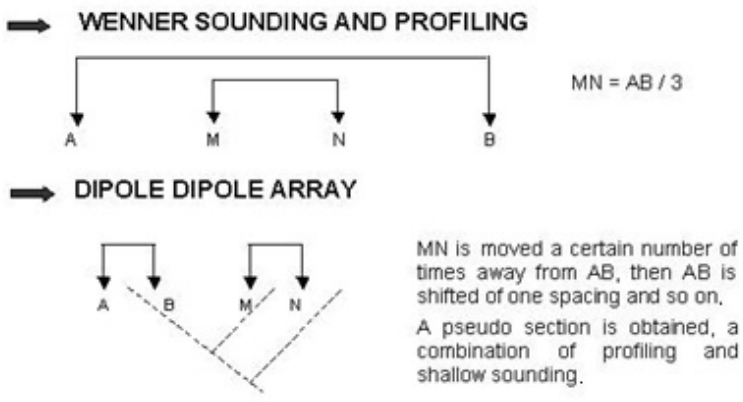


### 2.2.2 Capacitive coupled resistivity (CCR)

CCR surveying uses the earth as one conductor of a parallel plate capacitor. The transmitter and receivers are composed of two coaxial cables, or

dipoles. The transmitter sends a continuous-current sine wave through the dipole, polarizing the surrounding earth material; and the receiver measures the induced polarization, from which the resistivity can then be calculated. This system does not require inserted electrodes and can continuously collect pulsed readings at 1 sec intervals while traveling along the surface (Figure 16). Altering the separation between the transmitter and the receivers provides additional depths of survey. Again, we used RES2D to process the data; and this provides a cross section (pseudo-section) of the subsurface resistivity (x, z). Our study used the Geometrics OhmMapper TR5.

Figure 16. The OhmMapper system pulled by a snowmobile on a packed trail.

The measured output of the inversion data is in ohm-meters (ohm-m), and experience has shown that typically 0 to 100 ohm-m is thawed or possibly wet material, 100 to 1000 ohm-m is ice-poor frozen material and most probably coarse-grained material such as river gravels, and 1000 to 100,000 ohm-m is ice-moderate to ice-rich materials (Hoekstra et al. 1975). The ice complex and the syngenetic permafrost of the uplands of the Fairbanks area commonly have resistivity values in the range of 100,000

ohm-m and can be much higher. Comparisons of ohm-meter values between ERT (both 2- and 3-dimensional [2D and 3D]) and CCR, and even between repeat surveys in seemingly similar type of terrain using the same method, can vary. Noise (spikes) during collection can artificially raise or lower the overall apparent resistivity value used in the inversion process, affecting the acquired resistivity values. Although cleansing the data of spikes and dropouts prior to the inversion process is always conducted, often resistivity value differences are noted between similar surveys, sometimes by as much as an order of magnitude between same-day surveys.

## 2.3 Measurements

We constructed all transects in the same manner. We determined a beginning point (0 m) based on site topography, vegetation, surface water features, ground-ice expression at the surface, and evidence of thermokarst and kept the transects as straight as possible to minimize bias by excluding difficult or wet terrain or difficult vegetation. Variations in terrain type and overall condition determined the lengths of the transects; therefore, lengths were not the same for all transects. We flagged each transect every 10 m for fiducial markings to be used by the geophysics, drilling, and other surveys also being conducted.

Measuring the vertical extent of the active layer is easy but time consuming due to the point-scale nature of the measurement. A roughly 1 cm diameter graduated rod is pushed vertically downward through the vegetation, organic layer, and thawed soil to the point of refusal; and the penetration depth (i.e., vertical distance) is noted. This permafrost *frost probing* can yield heterogeneous results when undulating vegetation or soil features are present. For example, at all of our sites, tussocks composed of sedge material could be as much as 80 cm tall. Whether one probes through, along, or in between a tussock mass can greatly alter the frost probe depth at that location. To address this, we used a survey-grade GPS and installed markers at 4 m intervals along all four of our study-site transects. By probing alongside the markers during the summer, we were able to track the downward migration of the active layer with time. We also were able to consistently quantify active-layer development through a variety of vegetation and terrain materials.

Seasonal timing of geophysical measurements is often critical to successful surveys. Seasonal snowmelt water that is unable to fully drain due to a shallow active-layer thaw depth often prevents surveys from taking place

until mid- to late June in Interior Alaska. Resistivity surveys are not hampered by wet active-layer conditions; however, pooled water at the surface can compromise equipment and personnel safety. Wet conditions and rough terrain can be avoided by conducting surveying in the winter months. Mobility is often much easier on snow, and we found that thick snow cover does not hamper the system signal.

Our surveying plan consisted of completing at least one survey per technique at all transects. Many of these techniques have system-optimizing variables, and we conducted repeat surveys when changes in these variables were made. We performed CCR and ERT measurements along all four transects in mid- to late summer of 2013 and winter of 2014 at near-maximum active-layer thaw depth.

Our study also conducted borehole drilling to investigate subsurface conditions and to ground truth the interpretation of the resistivity measurements of the ground-ice state along each transect. We used a Geoprobe 7822 direct push technology (DPT) drill to acquire 5.7 cm diameter core samples. The DPT technique allowed us to acquire intact samples up to 1.5 m in length, letting us accurately assess the continuity and transitions of the ground-ice state. We used a combination of surface features (i.e., thermokarst affected terrain and vegetation changes and anomalous readings discovered in the geophysical survey imagery) to pinpoint the borehole locations. In total, we drilled 9 holes at Farmers Loop, 6 holes at Creamer's Field, and 4 holes at the Permafrost Tunnel.

# 3 Results

## 3.1 ERT

We conducted ERT surveys in the late summer months of August and September 2014 to coincide with dry surface conditions. All of our surveys used 1 m long electrodes spaced at 3 m. The cable was 82 electrodes long, capable of yielding a maximum single run length of 246 m. We conducted multiple runs on each transect with, generally, 120 m of overlap to ensure continuous survey depth along each transect. The survey depth achieved with this configuration was a nominal 50 m. We have not corrected for topography any of the ERT pseudo-sections.

We set up a 3-D ERT array at Creamer's Field in a 48 × 48 m grid with a 3 m electrode spacing. The location was at the beginning of the Creamer's Field single-line transect in the thermokarst area where drilling results and surface expression allowed us to determine the extent of an ice wedge at depth. We attempted to orient the array in a manner that would fully encompass the complete polygon.

### 3.1.1 Creamer's Field

Figure 17 is a composite of four overlapping ERT surveys along the entire length of the Creamer's Field transect. Ice-rich conditions were known to exist along the entire transect, with gravel beds dipping to greater depths at the end. The thermokarst at the beginning of the transect is moderately visible in the ERT survey, suggesting a deeper permafrost table in this area. We confirmed this by borehole drilling. Figure 18 is the 3-D ERT survey conducted at the start of the transect in the heavy thermokarst area. The ohm-meter index calculated during these inversions is more than 140,000 ohm-m; however, values of this extreme have been measured previously in very high ice content silts of the Fairbanks area.

Figure 17. The Creamer's Field transect composite ERT pseudo-section.

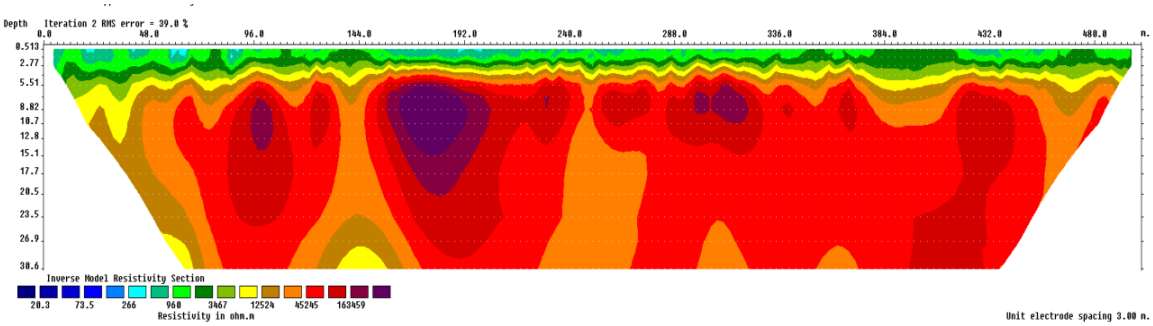


Figure 18. The Creamer's Field 3-D ERT collection.

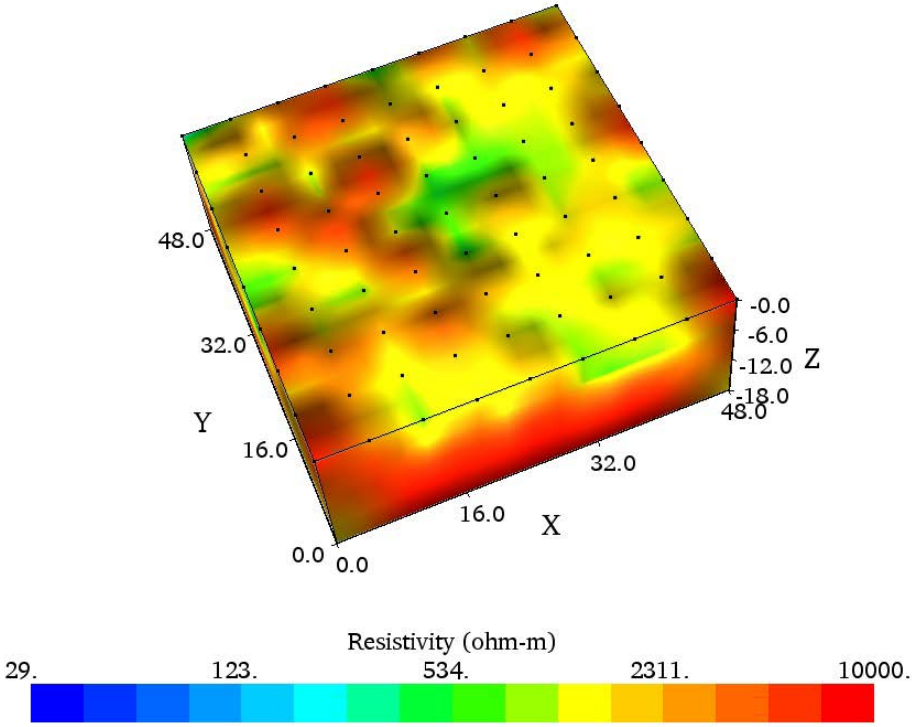


### 3.1.2 Farmers Loop

Figure 19 (T1) and Figure 20 (T2) show Farmers Loop composite ERT surveys. The thermokarst conditions noted at the beginning of each transect are clearly visible in these pseudo-sections.

Figure 19. The Farmers Loop T1 composite ERT pseudo-section.

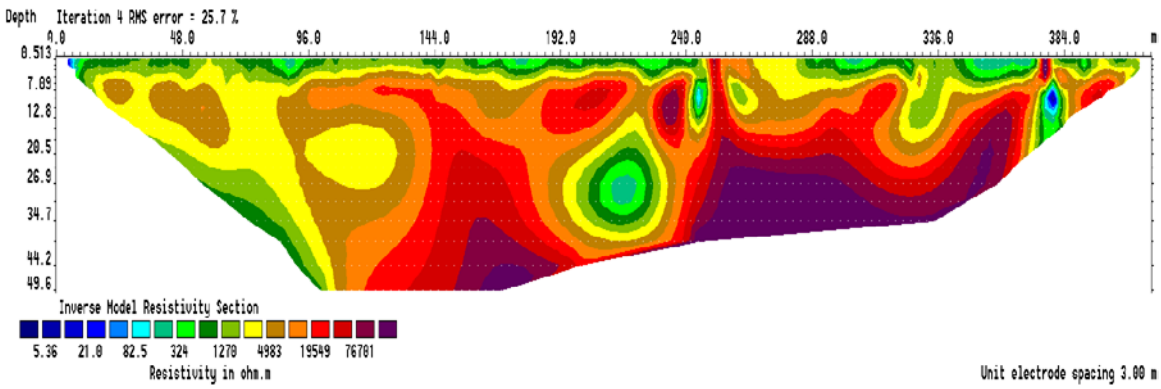


Figure 20. The Farmers Loop T2 composite ERT pseudo-section.

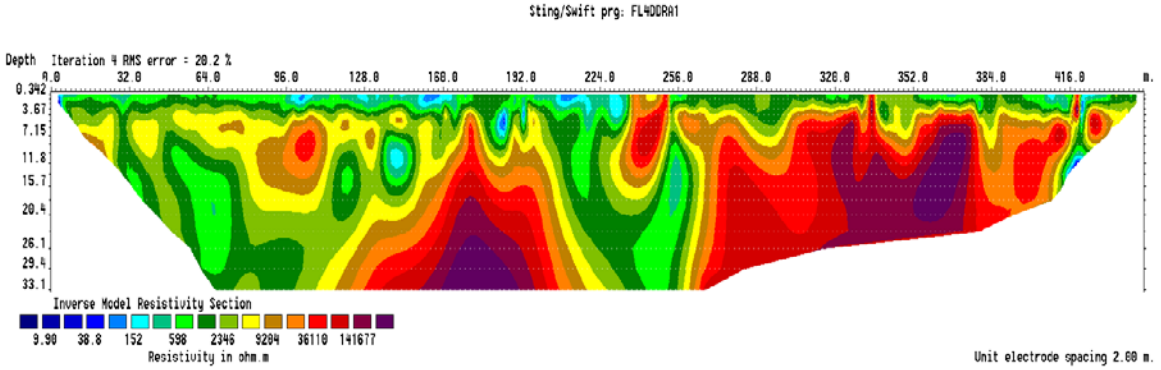


### 3.1.3 Permafrost Tunnel

Figure 21 shows the first section of the Permafrost Tunnel composite ERT survey. We encountered electronic problems with this transect, and repeat surveys were not attainable. This image is a good representation of the problems that can occur with ERT, as it is known that ice-rich conditions exist along this entire transect that are not clearly visible in the image.

Figure 21. The first section of the Permafrost Tunnel transect composite ERT pseudo-section.

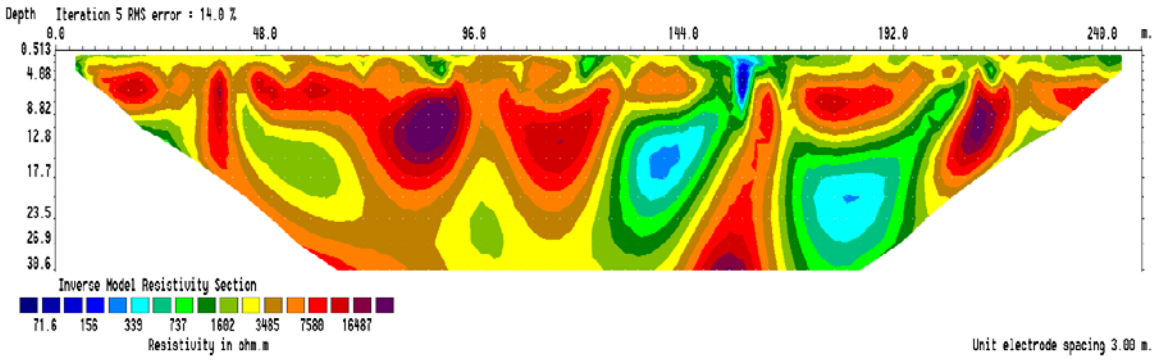

## 3.2 CCR

We conducted CCR surveys in mid-to late summer of 2013 (July–August), the spring of 2014 (May), and mid- to late summer of 2014 (July–August). Nearly all the surveys used 5 m dipole (2.5 m cables) and varying separation rope lengths of 2.5 m, 5 m, 12.5 m, 25 m, 30 m, 35 m, and 40 m. The notation to describe these configurations is dipole length in meters by rope separation length in meters (dipole length × rope separation length). In general, the shallow depths (shorter rope lengths) were consistent and could be completed with reliable and complete data collection. Longer rope lengths of 30 m to 50 m occasionally included spurious noise and dropouts requiring a resurvey or extensive filtering during post-processing. This was in part because of weak batteries, which prevented continuous connection while traversing relatively conductive terrain, such as thermokarst areas, with possibly high quantities of subsurface water. Figures 22 through 42 display pseudo-sections of the CCR data at all transects, and only a few have been corrected for topography (as noted).

### 3.2.1 Creamer's Field

Figure 22 illustrates the shallowest depth pass that we attained with this CCR system using the 5 m dipole and the shortest rope length of 2.5 m. This profile is topography corrected. The thermokarst area at the beginning of the transect is easily visible with low resistivity while the rest of the transect is moderately high at 10,000 ohm-m. This is a typical value for a shallow active layer with an organic, ice-moderate transition zone.

Figure 22. The Creamer's transect CCR with a 5 × 2.5 configuration.

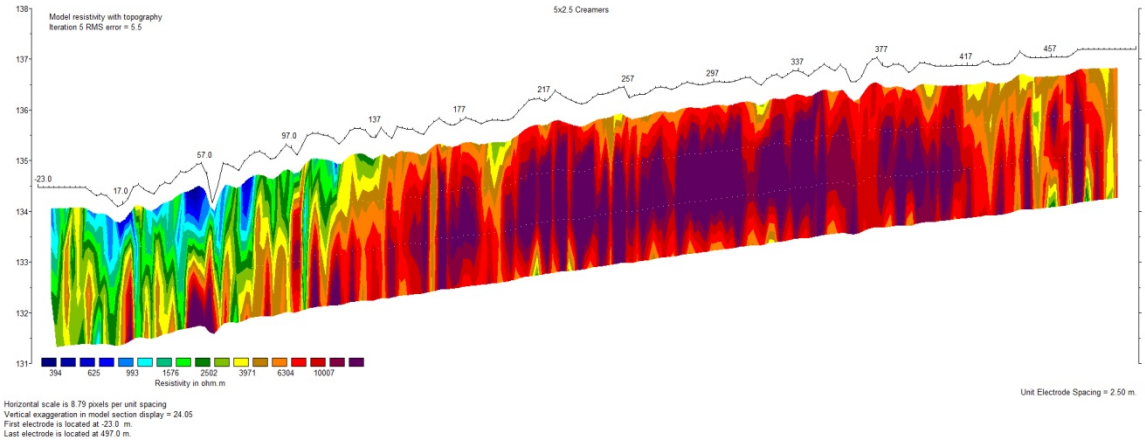


Figure 23 illustrates a typical mid-depth pass using this system. The permafrost soils at depth were more ice-rich, and we recorded higher values

around 30,000 ohm-m. The thermokarst region remains very visible at the beginning of the transect.

Figure 23. The Creamer's transect CCR with a 5 × 12.5 configuration.

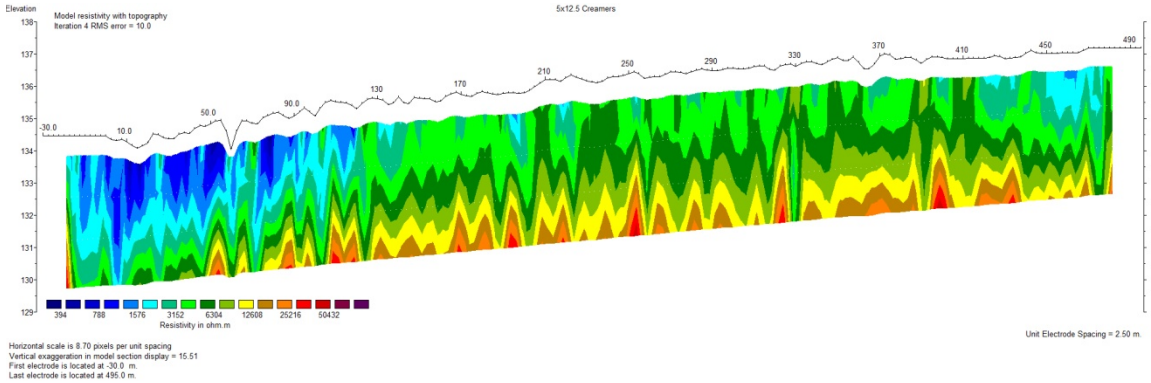


Figure 24 illustrates a deeper pass, and very ice-rich silts are beginning to be imaged at the 4 to 5 m depth. The value now approaches approximately 50,000 ohm-m. We confirmed the ice-rich peaks of high resistivity by drilling and correlating with the presence of surface visible ice-wedge polygons.

Figure 24. The Creamer's transect CCR with a 5 × 25 configuration.

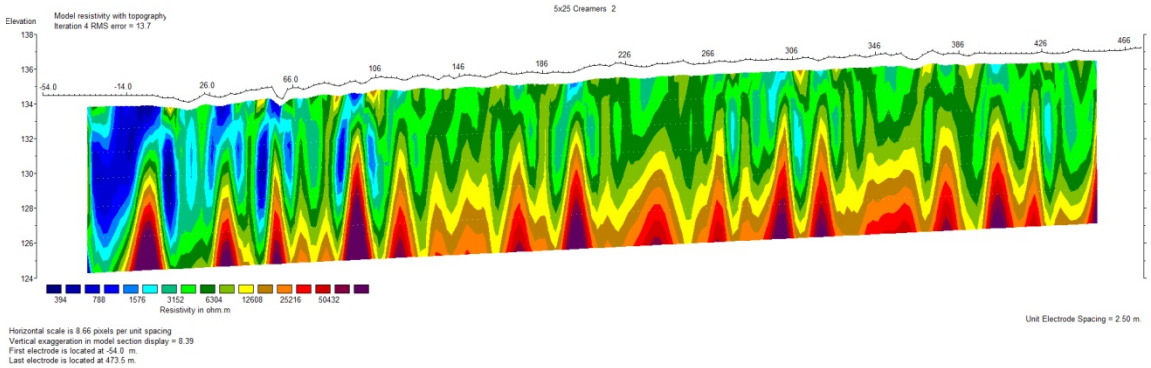


### 3.2.2 Farmers Loop

Figure 25 illustrates a shallow pass using the 5 m dipole and rope length of 5 m. Ice-moderate soils of the active-layer transient zone show readings at about 10,000 ohm-m.

Figure 25. The Farmers Loop T1 CCR with a 5 × 5 configuration.

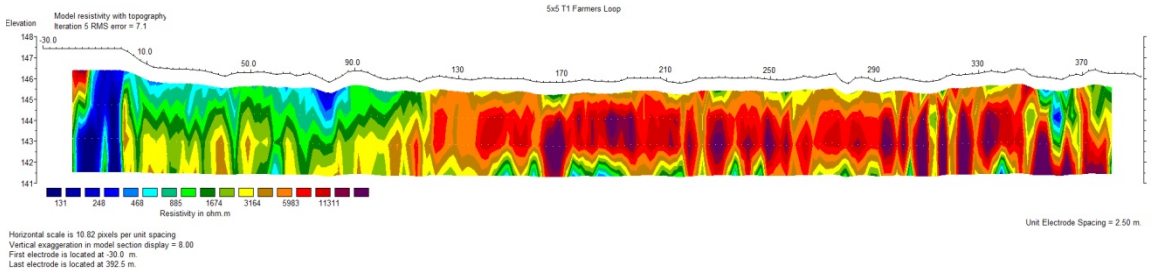


Figure 26 illustrates a middle-depth pass, and lower resistivity sediments existing at a shallower depth than the ice-rich transition zone are apparent. This was a typical occurrence, confirmed by drilling, where silt was found at moisture contents at saturation values.

Figure 26. The Farmers Loop T1 CCR with a 5 × 17.5 configuration.

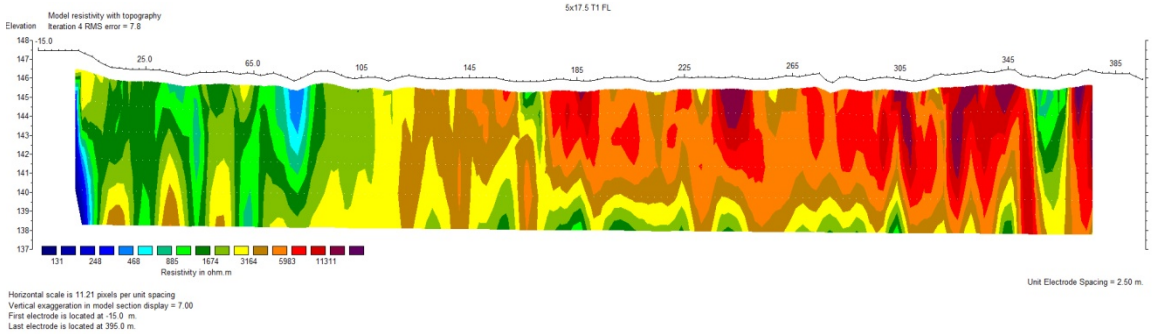


Figure 27 illustrates a deep pass using a 10 m dipole and a 35 m rope. These longer separation distances become problematic to maintain electronic lock between the transmitter and receiver, and fresh batteries often are needed to complete the survey. This image, in particular, highlights where values become distorted due to the many peaks induced in the data because of poor electronic lock of the system, illustrating what a poor survey set can produce.

Figure 27. The Farmers Loop T1 CCR with a 10 × 35 configuration.

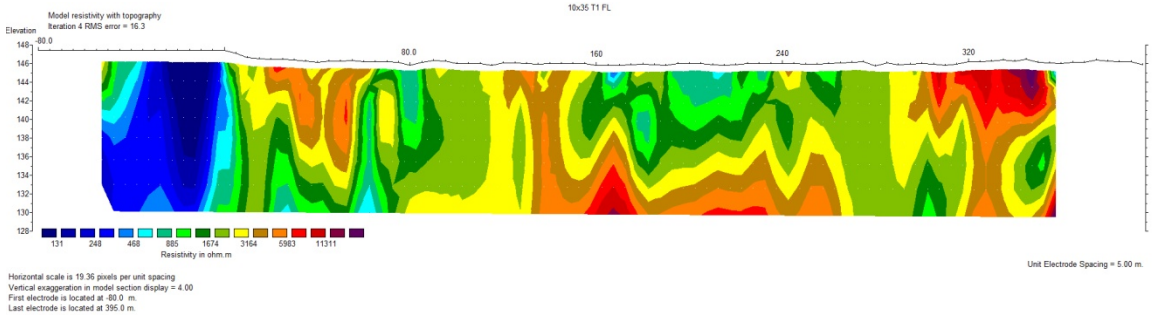

Figure 28 illustrates the shallow pass on T2 and with the same system geometry as on T1 (5 × 5). Again, the thermokarst at the beginning of the transect is visible, transitioning to the ice-moderate active-layer transition-zone values of approximately 9000 ohm-m.

Figure 28. The Farmers Loop T2 CCR with a 5 × 5 configuration.

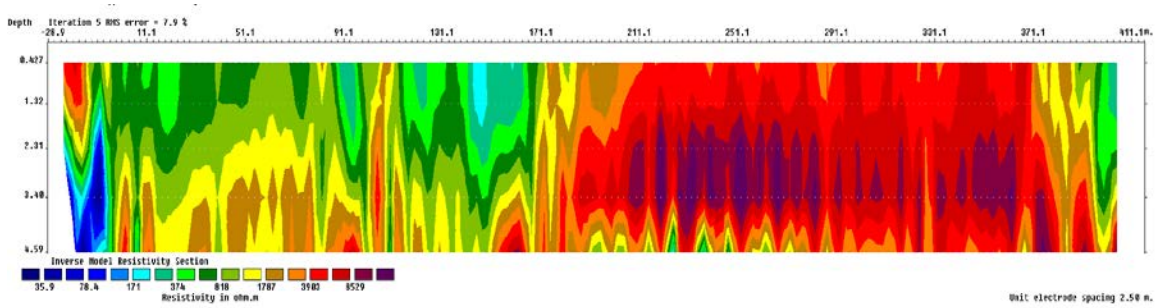


Figure 29 illustrates the mid-depth pass, and the results are much the same as for T1. Overall, the transect is becoming more resistive towards the end; and traces of lower ice-content soils at depth are apparent. We confirmed this by drilling, which identified the presence of deep ice-rich peats near the end of the transect; but elsewhere, ice-moderate silts and sandy-silts existed.

Figure 29. The Farmers Loop T2 CCR with a 5 × 17.5 configuration.

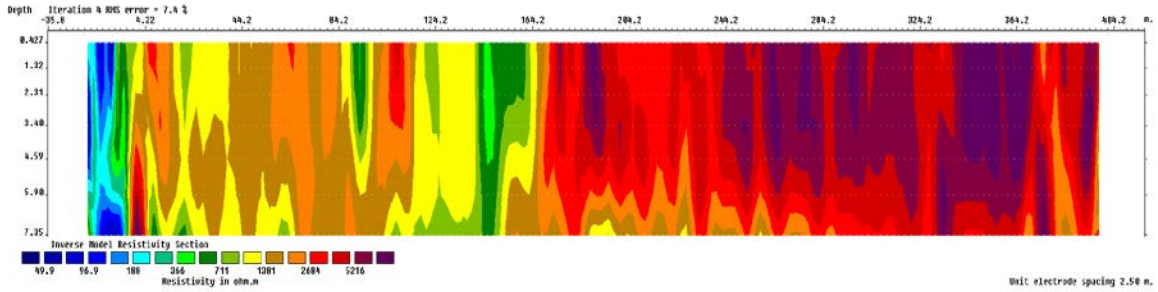


Figure 30 illustrates the deep pass. Unlike T1, however, this pass revealed better results as the survey achieved a more consistent electronic lock. We still encountered some problems, resulting in spikes in the data that corresponded to poor ohm-meter index results. This is visible in this image as values at approximately 3000 ohm-m.

Figure 30. The Farmers Loop T2 CCR with a 10 × 35 configuration.

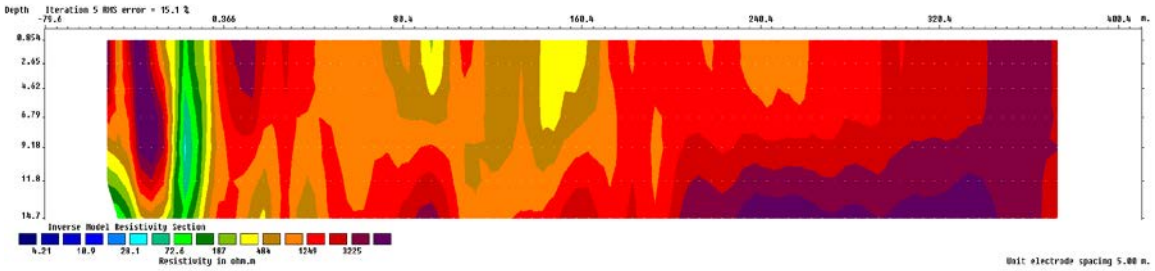


### 3.2.3 Permafrost Tunnel

Figure 31 illustrates a shallow pass at the Permafrost Tunnel transect. Visible in this pseudo-section is ice-poor to ice-moderate Holocene sediments existing in the near surface. The blue very low resistivity anomaly at about 150 m is where the transect crosses a trail leading up from the embankment where the Tunnels are constructed, up to the top of the Glenn Creek watershed. The next low resistivity anomaly at about 350 m corresponds to Glenn Creek. The ice-rich Pleistocene sediments at depth are just beginning to be imaged, and the high resistivity peaks are most likely ice-wedge polygons.

Figure 31. The Permafrost Tunnel CCR with a 5 ×5 configuration.

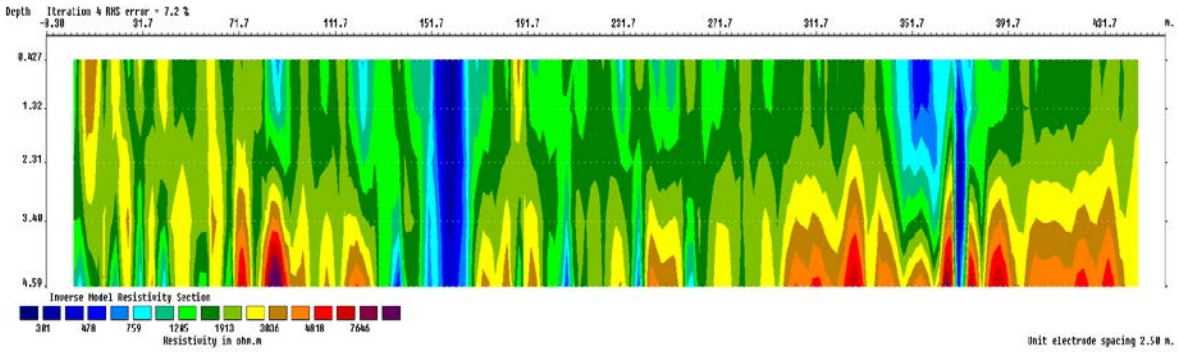


Figure 32 illustrates the mid-depth pass. Spikes produced during the survey distorted the ultimate inversion, producing a somewhat unrealistic image; however, the overall resistivity contrast is consistent and useful when compared with the shallow pass. This is an important note because, even when the system does not operate optimally, we still achieve contrast changes over the long transects that are very useful for interpretation, especially when used in conjunction with other passes and also with borehole drilling.

Figure 32. The Permafrost Tunnel CCR with a 5 × 17.5 configuration.

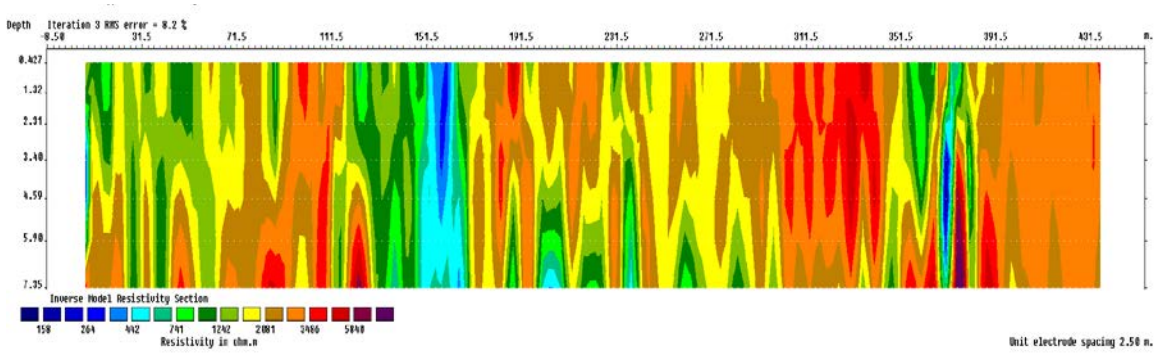


Figure 33 is a composite of four passes: the 5 × 5, 10 × 10, 10 × 30, and 10 × 50. All passes were conducted with 5 receivers, except for the third pass, which used only 3 receivers. We conducted this survey along the Glenn Creek watershed towards the escarpment at the Fox Permafrost Tunnel. We did not encounter any technical problems with the system, resulting in minimal errors during data collection and low root mean square errors during inversion. Here, we interpret the profile to delineate ice-poor Holocene near-surface soils with ice-rich Pleistocene soils and ice-wedge polygons at depth. Near the escarpment, the consistency of the ice-rich sediment was beginning to be lost; and this was confirmed by borehole drilling at the crest of the escarpment.

Figure 33. The composite Tunnel CCR survey conducted upslope from the tunnel portal.

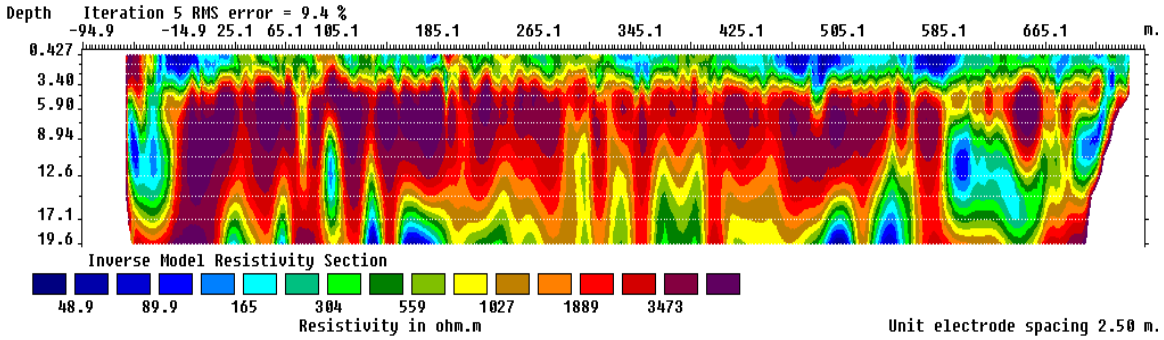


Figure 34 is a plot of the calculated resistivity vs. depth for the pseudo-section shown in Figure 29. This figure illustrates the inversion values for each receiver pass and is useful for comparing the groups of receiver passes, ensuring consistent data was collected for each depth. In this plot, we see a higher point density collected with the 5 × 5 geometry (first four lines and the sixth line); and that inconsistent overlap to the next depth grouping occurred between the 5 × 5 pass and the 10 × 12.5 pass (the separation

rope was too short). As a result, receiver #1 of the 10 × 12.5 pass is placed as the fourth line in the combined set, resulting in receiver #2 of the same set being the seventh line of data. If the geometry was properly aligned with proper rope lengths, receiver #2 would be the sixth line in the combined set. In this particular instance, the mis-overlap was not a problem as all the survey lines were consistent in the data, showing no spikes and only a minimal dropout in the deepest set, approximately three-quarters of the way through the survey.

Figure 34. A line plot of the calculated resistivity vs. depth for each receiver in the combined survey of Fig. 29.

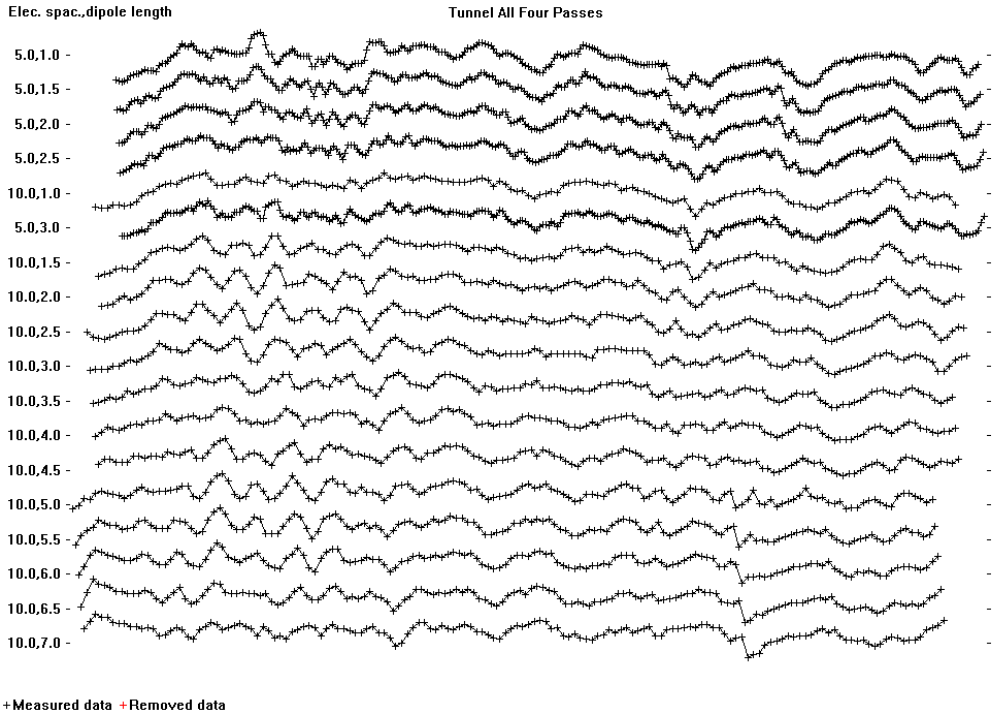


### 3.2.4 Farmers Loop with Creamer's Field long transect

Figure 35 illustrates a deep pass of a very long transect along T1 at Farmers Loop. The long pass starts at the beginning of the T1 transect and traverses through the end point and beyond to the west, ending very close to the end of the transect at Creamer's Field. At the beginning of the transect, ice-rich peats that are present at T1 and T2 are visible in the image, which transitions to relatively ice-poor silts, which end in a lake-strewn area near the Creamer's Field transect.

Figure 35. The Farmers Loop to Creamer's long transect (east to west) CCR with a 5 × 30 configuration.

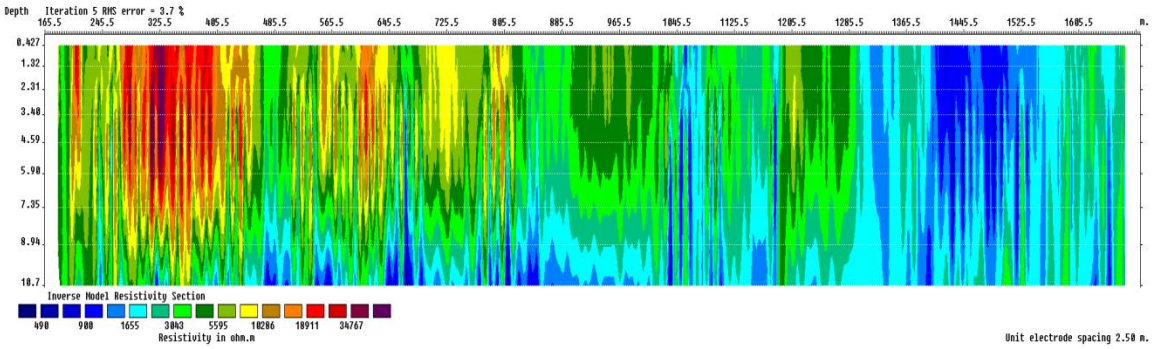


### 3.2.5 Image overlays

We overlaid CCR pseudo-sections with select satellite imagery collected over the Farmers Loop site. We used visible spectra from WorldView-2 satellite imagery collected on 21 May 2013 (Figure 36) and airborne LiDAR imagery collected May 2014 (Figure 37).

We overlaid CCR surveys for Farmers Loop T1 and T2 on Google Earth images (Figure 38 and Figure 39). It can be seen that the high resistivity area of the pseudo-section correlates very well with the tussock area containing ice-rich peats at depth. The low resistivity at the beginning of the pseudo-section correlates well with the presence of the thermokarst area at the beginning of each transect.

Figure 36. CCR T1, CCR T2, and CCR Farmers to Creamer's Field transects overlaid on visible spectra satellite image collected on 21 May 2013.

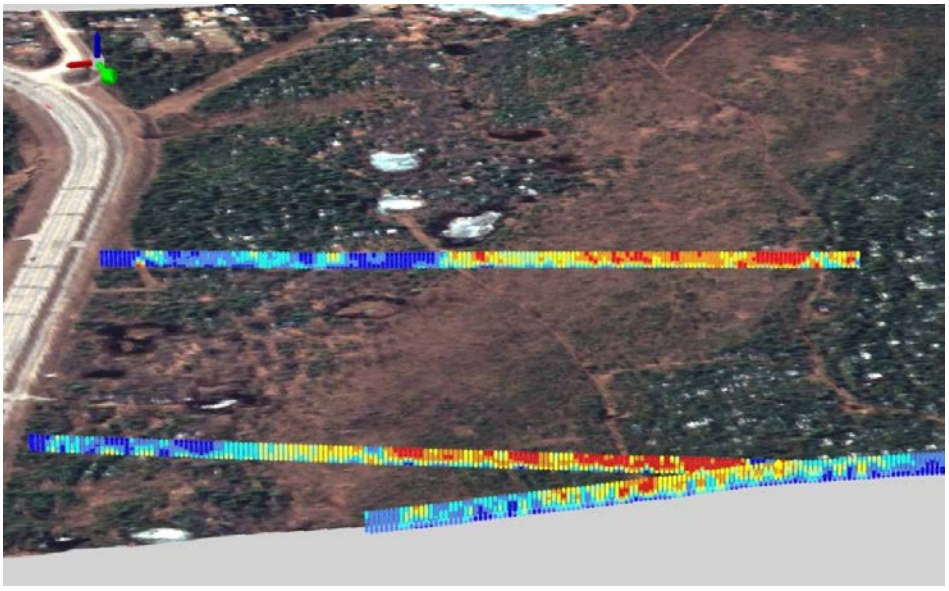

Figure 37. CCR T1, CCR T2, and CCR Farmers to Creamer's Field transects overlaid on an airborne LiDAR digital elevation model (DEM) collected May 2014.

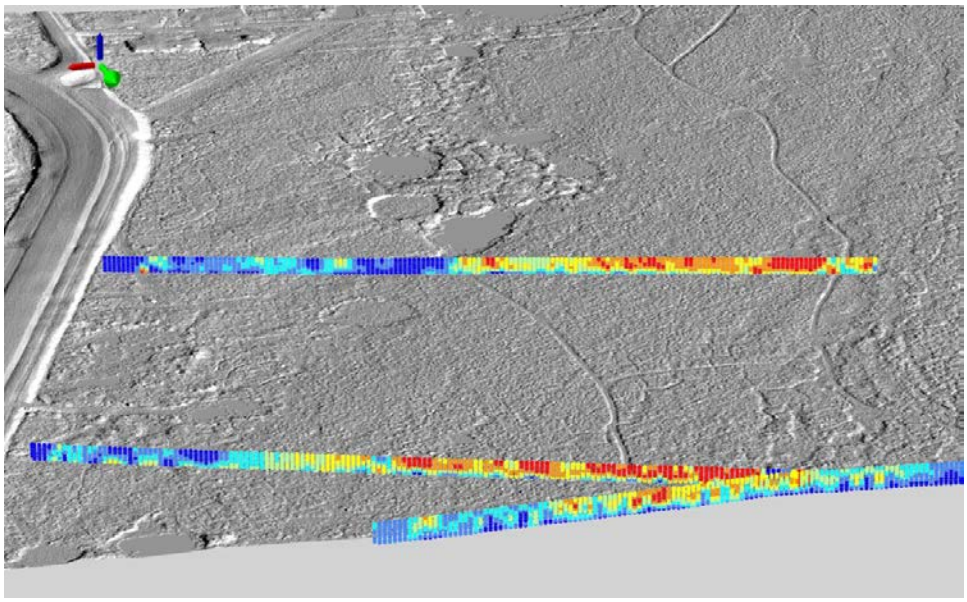

Figure 38. A combined CCR pseudo-section for T1 at Farmers Loop overlaid onto a Google Earth visible spectra image.

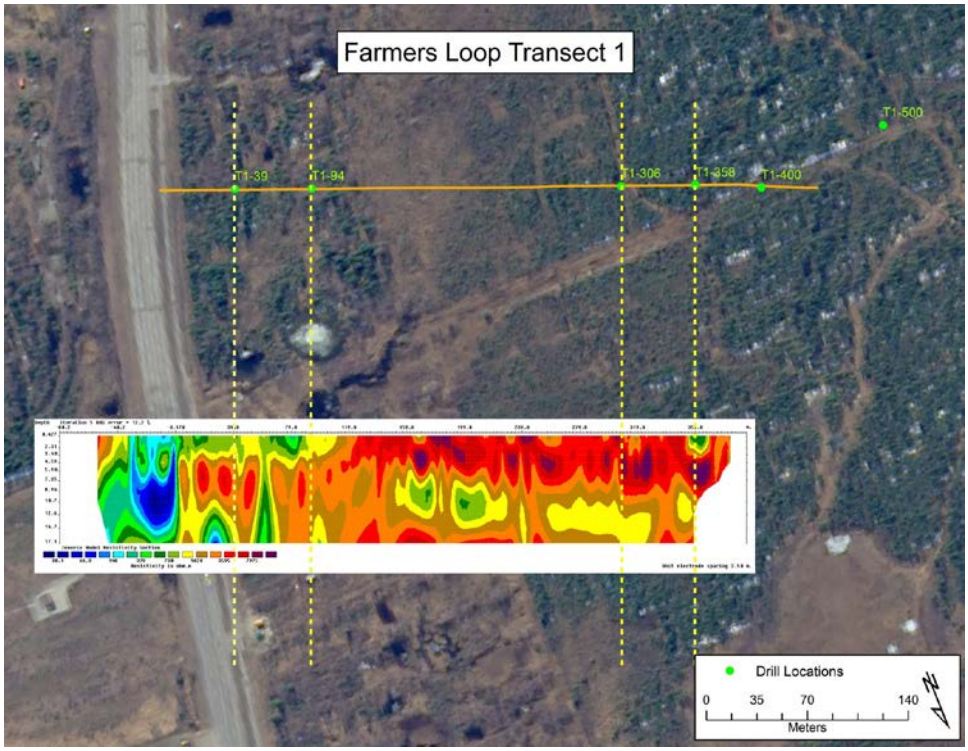

Figure 39. A combined CCR pseudo-section for T2 at Farmers Loop overlaid onto a Google Earth visible spectra image.

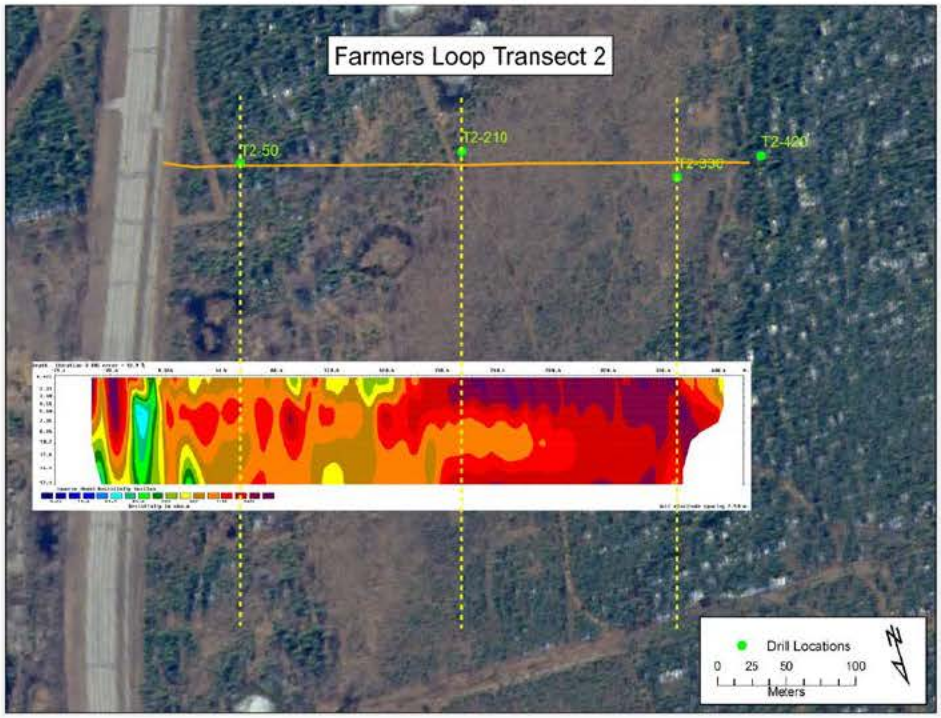


Figure 40 illustrates a long-distance CCR survey from Farmers Loop to Creamer's Field overlaid on a Google Earth image dated August 2013. Drilling performed on the Farmers Loop transects identified deep ice-rich peat deposits (down to 10 m) in the mixed tussock and dwarf deciduous forest (outlined in yellow dashed lines).

Figure 40. A combined long-distance CCR transect (*blue line*) overlaid on a visible spectra satellite image. *Red lines* are T1 and T2, and *yellow dashed lines* outline the mixed tussock and dwarf deciduous forest.

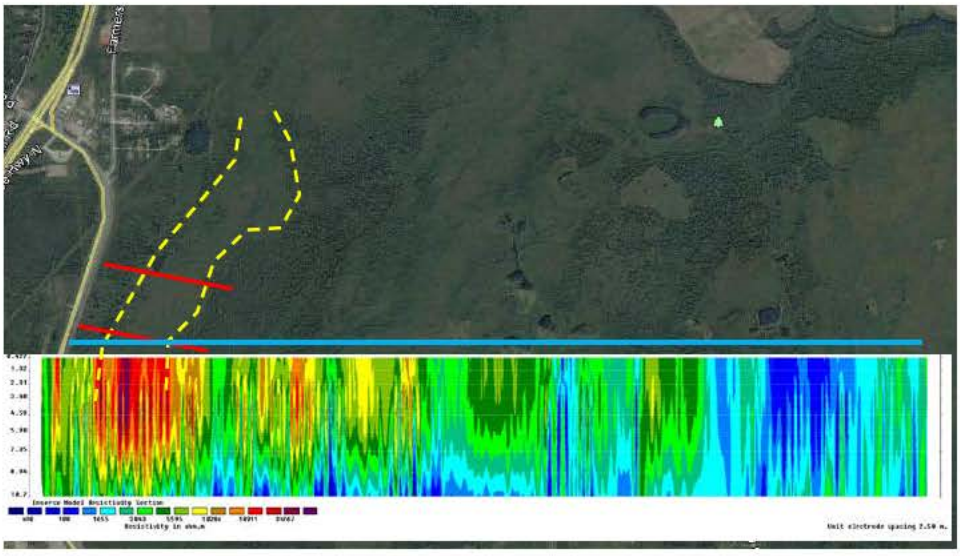

Figure 41 illustrates the ERT and CCR pseudo-sections acquired from Creamer's Field combined and overlaid onto a Google satellite image. Although we observed good correlation between the two measurement techniques, the ERT image does not show the detail apparent in the CCR image.

Figure 41. ERT and CCR pseudo-sections overlaid on a visible spectra satellite image at Creamer's Field.

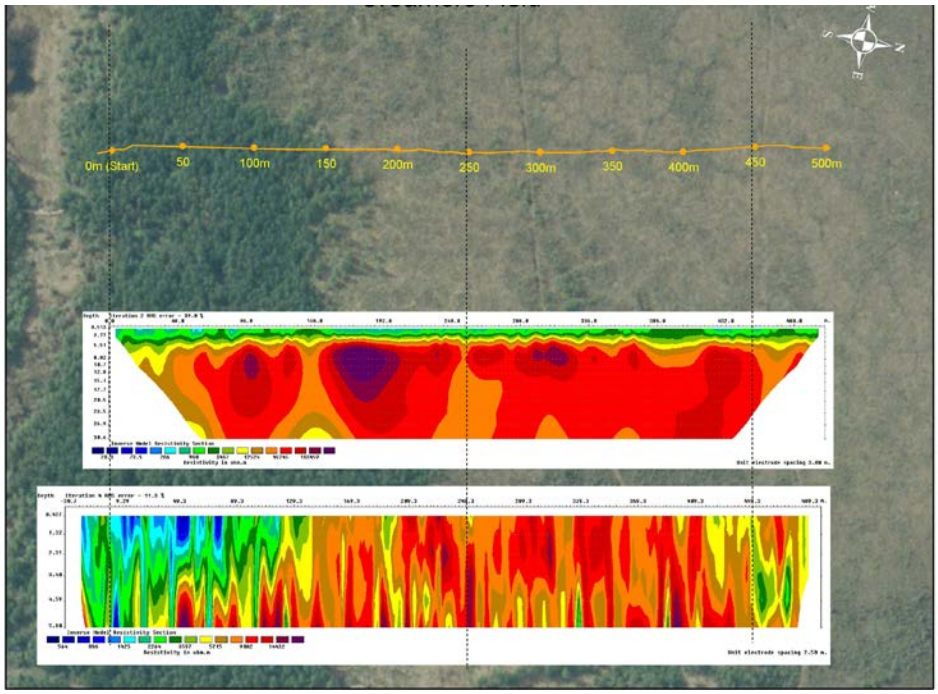


Figure 42 shows the CCR pseudo-section at the Permafrost Tunnel overlaid onto a Google satellite image and illustrates the nearly continuous ice-rich content of the Pleistocene sediments.

Figure 42. A CCR pseudo-section overlaid on a visible spectra satellite image at the Permafrost Tunnel.

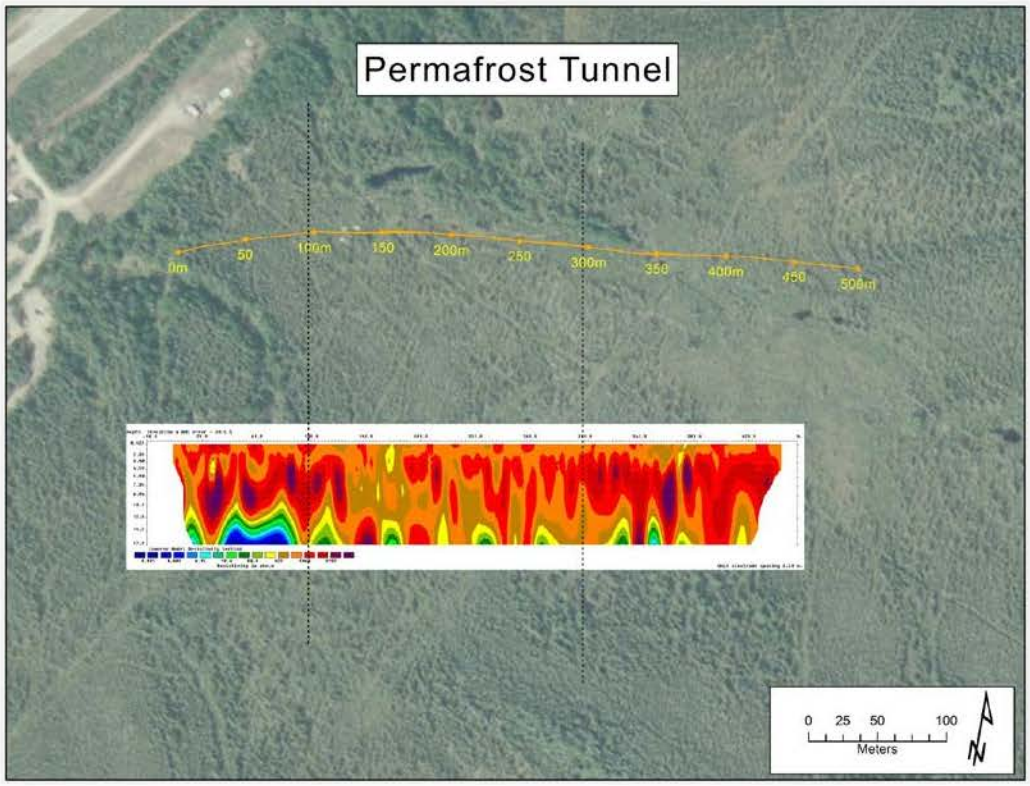

# 4 Discussion

Permafrost terrain, with respect to ground ice, is extremely heterogeneous. This prominent ground-ice heterogeneity is controlled by factors such as sediment particle size, organic content, topography, vegetation, slope aspect, elevation, water, and snow. In addition, ground ice is often characterized by definitive horizontal and vertical boundaries marking a transition from an ice-free or ice-poor state that immediately abuts an ice-moderate or ice-rich state. In many of the surveys conducted as part of this project, changes in ground ice condition and the presence of associated boundaries were clearly discernible. Boundaries were visible as definitive planes, as when measuring depth to the permafrost table, or as relatively large ice bodies (tens of meters).

Resistivity has the ability to read relative changes in ground-ice content. These changes are most readily imaged as larger (many meters) anomalous bodies, especially if these bodies are horizontally or vertically equal to or larger in size than the electrode spacing using ERT or the dipole length using CCR. Most often, these ground-ice changes are associated with the particle size of the sediment or rock; however, changes in ice content within the same size of host material can occur. In addition, thawed areas are easily discernible and register as pronounced low-resistivity anomalies. Conversely, areas of ice complex, with ice contents in the sediments often greater than 50% by volume, tend to register high resistivity across the transect.

In many instances, some aspect of the surface condition is also apparent at the boundaries where resistivity dramatically changes. This may be evident as a vegetation change, erosional or depositional feature, or as a surface-water drainage pathway. This is most evident in the CCR pseudosections that capture the thermokarst terrain at the beginning of T1 and T2 at Farmers Loop and at the beginning of the long transect from Farmers Loop to Creamer's Field.

In the case of CCR, increasing the point density of the measurements increases resolution over smaller areas; and this is most readily accomplished by reducing the speed of the system as it moves across the surface. Resolution can be increased in the ERT system by shortening the distance

between the electrodes. However, this also reduces the overall effective depth of the survey. Prior knowledge of the ground-ice conditions is beneficial to appropriately fine-tune the surveys for resolution efficiency. For example, if a transect many hundreds of meters in length is to be collected with the ERT system, spacing of the electrodes every meter will provide high resolution; but many separate surveys will be required to collect the entire length.

# 5 Conclusion

This project identified that resistivity surveys, ERT (galvanic) and CCR (capacitive coupled), have applicability in identifying changes in the ground-ice condition, which ultimately indicate overall ground-ice volume change. If ice features are larger than the dipole length of the system and the resistivity contrast to the adjoining material is large (i.e., a magnitude in variation or more), changes in resistivity values for that region will be imaged.

The ERT method is most applicable in collecting consistent data over a short transect (less than 200 m) and down to depths of less than 50 m. This method is time consuming, often taking several hours to install the electrodes and cables and to run the survey sequence. The CCR method is most applicable for collecting data over very long distances (tens of kilometers) in either rough or smooth terrain. Transect passes must be repeated to obtain multiple depth groupings that result in a full soil column of interest. We found the maximum depth of survey to be approximately 20 m.

The CCR resistivity technique allows quick surveys of large regions. In addition, by obtaining multiple transects in parallel, the technique provides imaging of subsurface permafrost terrain in a manner that has not been done previously. Airborne resistivity systems have the ability to map difficult and remote terrain very quickly, albeit a very expensive cost. The CCR and ERT methods attain high resolution with electrode separations of 1 m to 5 m while airborne methods use greater electrode separations of tens of meters, resulting in lower resolution.

Obtaining subsurface images that accurately determine relative changes in volumetric ground-ice content supports infrastructure operations and advances scientific studies of permafrost, a critical area of research under the context of global climate change.

# References

Bray, M. T., H. M. French, and Y. Shur. 2006. Further cryostratigraphic observations in the CRREL permafrost tunnel, Fox, Alaska. *Permafrost and Periglacial Processes* 17 (3): 233–243.

French, H. M. 1976. *The Periglacial Environment*. New York: Longman Inc.

Hamilton, T. D., J. L. Craig, and P. V. Sellmann. 1988. The Fox permafrost tunnel: a late Quaternary geologic record in central Alaska. *Geological Society of America Bulletin* 100 (6): 948–969.

Hoekstra, P., P. V. Sellmann, and A. Delaney. 1975. Ground and airborne resistivity surveys of permafrost near Fairbanks, Alaska. *Geophysics* 40 (4): 641–656.

Kanevskiy, M., Y. Shur, D. Fortier, M. T. Jorgenson, and E. Stephani. 2011. Cryostratigraphy of late Pleistocene syngenetic permafrost (yedoma) in northern Alaska, Itkillik River exposure. *Quaternary Research* 75 (3): 584–596.

Kanevskiy, M., D. Fortier, Y. Shur, M. Bray, and T. Jorgenson. 2008. Detailed cryostratigraphic studies of syngenetic permafrost in the winze of the CRREL permafrost tunnel, Fox, Alaska. In *Proceedings of the Ninth International Conference on Permafrost, 29 June–3 July, University of Alaska Fairbanks*, ed. D. L. Kane and K. M. Hinkel, 1: 889–894. Fairbanks, AK: Institute of Northern Engineering, University of Alaska Fairbanks.

Kneisel, C., C. Hauck, R. Fortier, and B. Moorman. 2008. Advances in geophysical methods for permafrost investigations. *Permafrost and Periglacial Processes* 19 (2): 157–178.

Lewkowicz, A. G., B. Etzelmüller, and S. L. Smith. 2011. Characteristics of discontinuous permafrost based on ground temperature measurements and electrical resistivity tomography, southern Yukon, Canada. *Permafrost and Periglacial Processes* 22 (4): 320–342.

Péwé, T. L. 1975. *Quaternary Geology of Alaska*. Washington, DC: U.S. Government Printing Office.

Shur, Y., K. M. Hinkel, and F. E. Nelson. 2005. The transient layer: implications for geocryology and climate-change science. *Permafrost and Periglacial Processes* 16 (1): 5–17.

Shur, Y., H. M. French, M. T. Bray, and D. A. Anderson. 2004. Syngenetic permafrost growth: cryostratigraphic observations from the CRREL Tunnel near Fairbanks, Alaska. *Permafrost and Periglacial Processes* 15 (4): 339–347.

Williams, P. J., and M. Smith. 1989. *The Frozen Earth—Fundamentals in Geocryology*. Cambridge, UK: Cambridge University Press.

Zhang, T., R. G. Barry, K. Knowles, F. Ling, and R. L. Armstrong. 2003. Distribution of seasonally and perennially frozen ground in the Northern Hemisphere. In *Proceedings of the 8th International Conference on Permafrost, 21–25 July, Zurich, Switzerland,* ed. M. Phillips, S. M. Springman, and L. U. Arenson, 2:1289–1294. Rotterdam, Netherlands: A.A. Balkema Publishers.

# REPORT DOCUMENTATION PAGE

*Form Approved*
*OMB No. 0704-0188*



| **1. REPORT DATE** *(DD-MM-YYYY)* | **2. REPORT TYPE** | **3. DATES COVERED** *(From - To)* |
|---|---|---|
| October 2015 | Technical Report/Final | |

**4. TITLE AND SUBTITLE**

Imaging of Ground Ice with Surface-Based Geophysics

**5a. CONTRACT NUMBER**

**5b. GRANT NUMBER**

**5c. PROGRAM ELEMENT NUMBER**

**6. AUTHOR(S)**

Kevin Bjella, Steve Arcone, and Thomas Douglas

**5d. PROJECT NUMBER**

**5e. TASK NUMBER**

**5f. WORK UNIT NUMBER**

**7. PERFORMING ORGANIZATION NAME(S) AND ADDRESS(ES)**

U.S. Army Engineer Research and Development Center (ERDC)
Cold Regions Research and Engineering Laboratory (CRREL)
Alaska Projects Office
Building 4070, 9th Street
Fort Wainwright, AK 99703

**8. PERFORMING ORGANIZATION REPORT NUMBER**

ERDC/CRREL TR-15-14

**9. SPONSORING / MONITORING AGENCY NAME(S) AND ADDRESS(ES)**

Headquarters, U.S. Army Corps of Engineers
Washington, DC 20314-1000

**10. SPONSOR/MONITOR'S ACRONYM(S)**

USACE

**11. SPONSOR/MONITOR'S REPORT NUMBER(S)**

**12. DISTRIBUTION / AVAILABILITY STATEMENT**

Approved for public release; distribution is unlimited.

**13. SUPPLEMENTARY NOTES**

**14. ABSTRACT**

Electrical properties of earth materials have profound differences due to the phase change of water to ice. This contrast is useful when using electro-magnetic methods to study permafrost terrains where frozen and thawed materials are intermixed. Engineering and science are in need of efficient, non-invasive tools for imaging ice and sediment composition. Borehole information is often used to map ice in permafrost terrains; but it is time consuming, expensive, and can lead to over- or underquantification of ground ice. Advances in computing power have led to refined surface-based geophysical methods, and the goal of this study was to determine if the latest commercial technologies or system were promising for imaging ground ice and associated features and to compare the results across a variety of permafrost terrains.

Electrical Resistivity Tomography (ERT), in particular, has been effective for imaging ground ice. ERT measures the ability of materials to conduct or resist an electric current. A variation of this method, capacitive coupled resistivity (CCR) offers the ability for continuous data collection while moving across the landscape at scales of meters to kilometers. This greatly enhances the cost efficiency, applicability, and overall usefulness of the techniques and provides the ability to view variations in permafrost ice content on these larger scales.

**15. SUBJECT TERMS**

Ground ice
Ground resistivity
Non-intrusive geophysical methods
Permafrost
Terrain characteristics

| **16. SECURITY CLASSIFICATION OF:** | | | **17. LIMITATION OF ABSTRACT** | **18. NUMBER OF PAGES** | **19a. NAME OF RESPONSIBLE PERSON** |
|---|---|---|---|---|---|
| **a. REPORT** | **b. ABSTRACT** | **c. THIS PAGE** | | | **19b. TELEPHONE NUMBER** *(include area code)* |
| Unclassified | Unclassified | Unclassified | SAR | 47 | |